

---

---

# Physical Modeling and Optimisation of a EMT 140 Plate Reverb

---

---

Master's Thesis  
Riccardo Russo

Aalborg University  
Architecture, Design and Media Technology





**AALBORG UNIVERSITY**  
STUDENT REPORT

**Architecture, Design and Media  
Technology**  
Aalborg University  
<http://www.aau.dk>

**Title:**

Simulation and Optimisation of a EMT  
140 Plate Reverb

**Theme:**

Modeling Physical systems

**Project Period:**

Spring Semester 2021

**Participant(s):**

Riccardo Russo

**Supervisor(s):**

Michele Ducceschi  
Stefania Serafin

**Copies:** 1

**Page Numbers:** 65

**Date of Completion:**

May 28, 2021

**Abstract:**

The EMT 140 is a plate reverb that exploits the vibrations of a metallic plate to simulate reverberation. It was an industry standard in the 60s and 70s, and its sound is still widely appreciated nowadays. In this work, a physical model of the EMT 140 is developed, by adopting a modal approach. First, a modal decomposition of the plate vibration is performed; then, a physically-based model for damping is presented, based on previous works, including a simulation of the controllable damper present on the real unit. The modes equations then are discretised with an exact numerical integrator. As physical models are quite computationally expensive, here an optimisation technique is also presented, based on linear least squares. Results show that the optimisation could reduce the computational time by 80%, while still maintaining a high sound quality.

*The content of this report is freely available, but publication (with reference) may only be pursued due to agreement with the author.*



# Contents

<b>1</b>	<b>Introduction</b>	<b>1</b>
1.1	Artificial Electromechanical Reverberation . . . . .	1
1.1.1	The EMT 140 Plate Reverb . . . . .	3
1.2	Basics of Room Reverberation . . . . .	4
<b>2</b>	<b>State of the Art</b>	<b>7</b>
2.1	Delay Networks . . . . .	8
2.2	Convolution . . . . .	9
2.3	Physical Modeling . . . . .	10
2.3.1	Physical Modeling for Plate Reverberation Simulation . . . . .	11
2.4	Neural Networks . . . . .	13
2.5	Commercial Plugins . . . . .	13
2.5.1	Universal Audio EMT 140 Classic Plate Reverberator . . . . .	13
2.5.2	IK Multimedia CSR Plate Reverb . . . . .	14
2.5.3	Waves Abbey Road Reverb Plate . . . . .	14
2.5.4	Arturia Rev PLATE-140 . . . . .	14
2.5.5	Valhalla Plate . . . . .	16
2.5.6	Physical Audio PA1 Dynamic Plate Reverb . . . . .	16
2.5.7	UVI Plate . . . . .	16
2.6	Project Goal . . . . .	17
<b>3</b>	<b>Plate Model in the Continuous Domain</b>	<b>19</b>
3.1	Kirchhoff-Love Model . . . . .	19
3.2	Dispersion Relation and Wave Propagation . . . . .	20
3.3	Loss and Tension . . . . .	21
3.4	Damping . . . . .	22
3.4.1	Thermoelastic Damping . . . . .	22
3.4.2	Radiation Damping . . . . .	23
3.4.3	Damping induced by a Porous Medium . . . . .	24
3.5	Modal Analysis . . . . .	28

<b>4</b>	<b>Discrete Simulation</b>	<b>31</b>
4.1	Finite Difference Schemes Synthesis . . . . .	31
4.2	Simple Harmonic Oscillator . . . . .	33
4.2.1	Accuracy of the SHO . . . . .	34
4.2.2	Exact Scheme for the SHO . . . . .	34
4.3	Lossy Oscillator . . . . .	35
4.3.1	Exact Scheme for the Lossy Oscillator . . . . .	36
4.3.2	Forcing . . . . .	37
4.4	An Update Equation for the Modes . . . . .	38
<b>5</b>	<b>Optimisation</b>	<b>39</b>
5.1	Least Squares Regression . . . . .	39
5.1.1	Multiple Explanatory Variables . . . . .	41
5.1.2	Complex Variables . . . . .	41
5.2	Modes Optimisation . . . . .	42
5.2.1	Frequency Response . . . . .	42
5.2.2	Least Squares . . . . .	43
<b>6</b>	<b>Results &amp; Evaluation</b>	<b>47</b>
6.1	Measurements Setup . . . . .	47
6.2	Frequency Bands & Modes Rejection . . . . .	48
6.2.1	Running Times . . . . .	50
6.3	Technical Evaluation . . . . .	50
6.3.1	Bark Bands . . . . .	51
6.3.2	Linear Bands . . . . .	52
6.4	Perceptual Test . . . . .	53
6.4.1	Survey Results . . . . .	54
6.5	Final Considerations . . . . .	56
<b>7</b>	<b>Conclusion &amp; Future Work</b>	<b>59</b>
	<b>Bibliography</b>	<b>61</b>

# Preface

Aalborg University, May 28, 2021



---

Riccardo Russo  
<rrusso19@student.aau.dk>



# Chapter 1

## Introduction

Acoustic reverberation can be defined as the persistence of a sound in an acoustic space, after the source was stopped. It is a natural phenomenon, caused by the reflection of the acoustic pressure waves against rigid obstacles. Each reflection causes a modification in the frequency content of the sound, depending on the physical characteristics of the environment; thus, the reflected waves which finally reach the listener's ears are slightly different from the ones that were emitted by the source, and arrive after some time (delay) [1]. These two aspects have a role in the identification of the environment characteristics and the localization of the sound source from the human brain.

### 1.1 Artificial Electromechanical Reverberation

Since reverberation is ubiquitous in every day life, its presence and its characteristics are very important, particularly in the context of music. For thousands of years, reverberation has been a primary concern when designing theatres and concert halls, in fact, too long or too short reverberation time can cause a performance to sound chaotic or too dry [2]. The need for artificial reverberation, which could simulate a room acoustic, emerged for the first time in the context of music recording. It was the moment in history when music could be played in a place different from the one where it was listened; therefore, a number of locations dedicated specifically to recording music started to arise: the recording studios. Soon though, it became clear that sounds recorded in these places lacked the spatiality of live music. Studios work with many different kinds of music; however, the recording rooms are always the same and the acoustic characteristics cannot be varied. In addition, the close placings of microphones cut a great part of the room reverberation in any case. To overcome these issues, a number of techniques were developed to artificially simulate the characteristics of a real environment, the first of which were based on electromechanical principles.

The first artificial reverberator, invented in 1926 by RCA, is the *echo chamber* [3]. It was first developed for broadcasting applications and, after a few years, its use was extended to musical applications [1]. It consists of an empty room, where the walls are covered with an acoustic reflective material and are built to lack parallel surfaces, in order to avoid unwanted resonances. A pre-recorded sound is reproduced inside the room by a speaker placed at a corner, a position which ensures the excitation of a large number of modes. Microphones are then placed in various positions, according to the wanted echo quantity, and pick up the resulting sound pressure. Dampers can be also placed at walls, to obtain a rudimental control over the reverberation time. The original (dry) and reverberated (wet) sounds are then mixed together by the sound engineer in the desired proportions. The echo chamber was the first device which allowed to apply reverb to a recorded sound without having to move from a recording studio, however, it presented some inconveniences. For instance, the reverberation time was fixed, and the construction of such an apparatus required a dedicated room.

Spring reverberation was invented in 1928 by the Bell Labs [4]. It consists of a transducer which converts the electrical sound signal into physical displacement, putting a spring (or multiple springs) into vibration. The springs movement is then captured by a coil, which converts it back to an electrical signal. The resulting sound is perceived as reverberant because the mechanical waves bounce back and forth multiple times inside the coil, thus producing echoes. The higher the number and the variety of springs, the more realistic the effected sound is, as the echoes times is more variable. Springs can be put in series or parallel, or placed in liquids such as oil to obtain different effects. This reverb system presents a big advantage over echo chambers: it can be very small and portable, to the point that Laurens Hammond developed his version of it to place it inside his organ, and Leo Fender included it inside the Twin Reverb amplifier [2]. On the other hand, the springs natural frequencies of vibration produce a typical "twang", which makes the spring reverb very distinguishable from natural reverberation.

The first plate reverberator was invented in the late 50's by the German company Elektromesstechnik (EMT). The functioning is similar to that of the spring reverb, except that the coil is replaced by a metallic plate. A punctual transducer, placed near the center of the plate, converts the sounds signal into movement and puts the system into vibration. A pair of accelerometers then measure the displacement of the plate in two different positions, providing a stereo effected sound. The small dimensions (compared to an echo chamber) of the plate reverb allowed a single recording studio to run many of these devices in parallel in different rooms, without interfering with each others, meaning that it was possible to work on different instruments or songs at the same time. Moreover, the quality of the sound obtained was so much appreciated that plate reverberation became an industry standard in the 60s and 70s.



Figure 1.1: An EMT 140 Plate Reverb (Source: [5])

### 1.1.1 The EMT 140 Plate Reverb

Even though many different versions of this effect were produced, the most popular was undoubtedly the EMT 140, made by EMT; for instance, it is the only reverb used on Pink Floyd's *Dark Side of the Moon* [6]. The reverberant element of the unit consists of a  $2\text{ m} \times 1\text{ m}$  rectangular steel plate, with a thickness of 0.5 mm. The plate is suspended in a chassis made of tubular steel, and held under tension by two steel wires at each corner: one horizontal and one vertical. As described above, the plate is excited by an electrodynamic actuator, and the reverberated signal is captured by two accelerometers, which measure the system displacement. To provide control over the reverberation time, a porous panel is placed near and parallel to the plate, with a distance that can be varied between 11 and 66 mm. Damping is increased by approaching the panel to the plate. In fact, the presence of the porous material modifies the impedance in the nearfield of the plate, thus increasing radiation. More details on the damping functioning will be provided in chapter 3.

Despite many progress on artificial reverberation have been made since the EMT 140 was invented, its iconic sound is still sought after by musicians and sound engineers. Nevertheless, the unit is too bulky for the majority of studios nowadays (it weights around 240 kg), and needs constant maintenance. For this reason, accurate digital simulations of this reverb are highly desirable.

The matter of creating digital models of existing analog devices is called *Virtual*

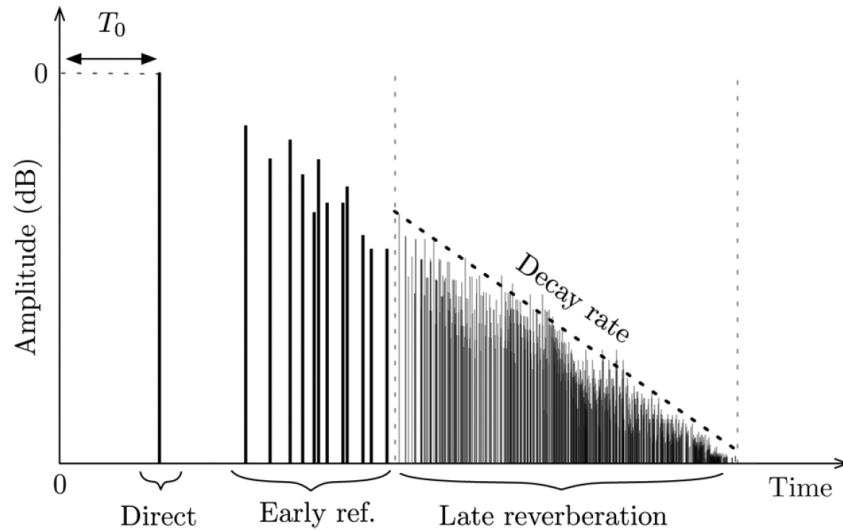


Figure 1.2: Schematic of a generic room impulse response. (Source: [1])

*Analog* (VA) modeling. With VA, it is possible to get access to the sound of instruments which are too rare or expensive to be bought. In addition, once developed, VA simulations do not need to be manufactured or maintained. Analog devices are difficult to model; they possess a component of randomness which is intrinsic in real objects, and difficult to reproduce digitally. Moreover, the appreciated sound characteristics are usually given by nonlinear components, and creating a mathematical description of those is not always an easy task. Nevertheless, VA is getting more and more accurate as time goes on.

In this work, a method for virtual analog simulation of the EMT 140 plate reverb is implemented. The model is based on physical measurements, in a tentative to capture most of the iconic sound nuances. In addition, a technique for computational optimization is proposed, which allows to reduce the CPU load needed by the model.

## 1.2 Basics of Room Reverberation

This section provides a brief illustration of the basics of natural reverberation, which will later come in handy for understanding the main differences between plate and room reverb, and the reasons which make the latter so iconic. The reverberation characteristics of an environment depend on many factors such as dimensions and material. For example, the big empty spaces of a cathedral will determine long delays between the arrival of the source sound and the reflections, and the stone walls will produce a large amount of late reflections, which will form a background ambience. On the contrary, a small room with walls made of

an absorbent material such as wood will be very dry, causing the source sound to decay soon.

Whether we deal with a concert hall or a small recording studio, the reverberant characteristics can be described by the same model. Sound reaches the listener in stages, as shown in Figure 1.2. After a first delay  $T_0$ , the *direct sound* arrives: this is the signal directly emitted from the source and provides information on the emission location. The direct sound is followed by the *early reflections*, which are made of waves reflected only few times by nearby objects. These provide information on the surrounding space: the shape and the material of the boundaries. In the meantime, waves keep reflecting through space, generating additional reflections which form a dense echo: this stage is called *late reverberation* and it makes up the tail of a reverb. The evolution of the late reverberation power over time is called *reverberation time*. Sabine [7] defined it as the time necessary for the sound to experience a 60 dB decay and denoted it  $T_{60}$ . Moreover, Sabine was the first to experimentally prove the close link between the  $T_{60}$ , the size of the acoustic space and the absorbing characteristics of the walls materials, providing an empirical relation which is still the basis for modern studies on reverberation [8, 9].



## Chapter 2

# State of the Art

The previous chapter illustrated the fundamentals of natural reverberation and provided an overview of the first methods that were invented for trying to artificially reproduce it. Due to technological limitations (electronics was in an early stage of development, or did not even exist yet), all the solutions previously described make use of electromechanical components to induce vibrations in a medium and capture them back. For instance, echo chambers work by exciting a volume of air, while plate reverb employs the displacement of a metallic medium. As such, the result is highly dependent on external physical conditions, and obtaining an identical result many times is not that obvious. Moreover, since the vibrating medium is not air, spring and plate reverb have a characteristic sound which is different from the one produced by natural reverberation (even though this is one of the reasons for which their popularity continues nowadays). These problems, along with the fact that electromechanical systems are fragile, complicated (if not impossible) to move and require time consuming maintenance, created the need for more reliable systems. The answer to these problems was provided by electronics and the invention of digital reverberation, which guaranteed reproducibility, cheap systems and portability.

This section will provide an overview of the different digital reverberation techniques that were developed through the years. Since this work aims to implement a simulation of the EMT 140 plate reverb, only the methods suitable (or already used) for this purpose will be revised. The different techniques can be divided into four main families: *Delay Networks*, *Convolution*, *Physical Modeling* and *Neural Networks*. Some of these categories can overlap, however, this distinction will be useful to group them in the next pages. At the end of the chapter, a list of commercial plugins which emulate plate reverberation will be illustrated.

## 2.1 Delay Networks

The earliest digital reverberation techniques are based on delay networks. The idea behind these approaches is to model the room reflections with delay lines to implement the time differences between the arrival of the different waves (echoes). Filters are then used to shape the energy losses that occur during reflections. These methods are among the most efficient ones and, therefore, still studied nowadays.

The first studies on digital reverberation were carried out by Schroeder in the 60s [10, 11]. In [10], together with Logan, they proposed to place comb filters in series to simulate the arrival of the sound waves. A feedback comb filter is implemented by using a delay line, therefore, the resulting output of the reverb is perceived as several copies of the input, with a decaying level. If the delay is sufficiently short, the comb filter nature of the reverb emerges and, as a consequence, a pitched sound can be heard; in fact, it is possible to hear the normal modes of vibration of the filter. In a second work [11], Schroeder and Logan proposed the use of allpass filters in place of comb filters. The advantage of doing this is that, by nature, allpass filters do not change the amplitude of the frequency response. As a result, the presence of normal modes of vibration, typical of comb filters, can be avoided; for this reason, allpass reverbs are said to be "colorless". In the late 70s, Moorer [12] reviewed Schroeder's works and enhanced them by tuning the filters parameters to simulate the geometry of various existing rooms. In addition, he added a one-pole lowpass filter to Schroeder's models, in order to simulate the absorption of high frequencies by air.

Feedback Delay Networks (FDNs) were first proposed by Stautner and Puckette [13] as a way to generalize and "vectorize" networks of feedback comb filters. Later, Jot and Chaigne [14] formalized the algorithm, providing a structure which is still used nowadays [1]. FDNs essentially consist of a set of parallel delay lines of different sizes and a feedback matrix, which couples the delay outputs together. A simple FDN structure is shown in Figure 2.1. Jot and Chaigne started working on these structures as it became clear that they could help in overcoming one of the biggest limitations of Schroeder reverberators: low time density, i.e. the number of echoes per second. In particular, they realized that the method previously proposed by Stautner and Puckette could build up high time densities by using only few delay lines. In addition these algorithms are usually made to be lossless [15], meaning that no energy is lost during the delays; this allows to implement decay using absorbent filters, thus providing control over the frequency dependent reverberation time, something which was not possible with Schroeder's structures. The characteristics illustrated above, along with the lightweight and efficient design, make FDNs still widely appreciated and studied algorithms for modeling room impulse responses [16, 17]. FDNs have been used in the context of plate reverberation simulation by Abel [18]. In this work, a hybrid approach was employed,

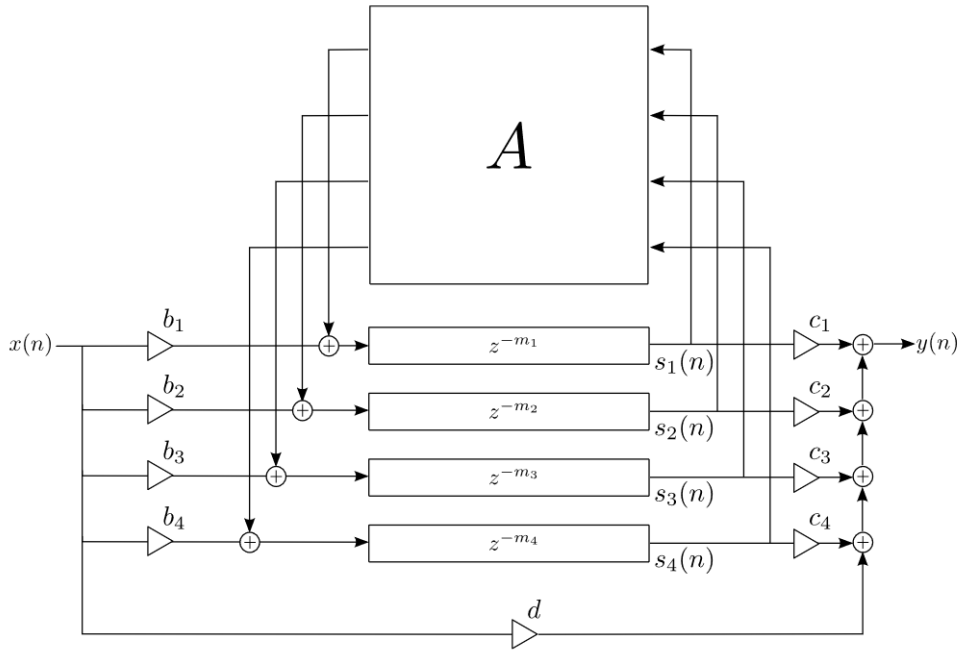


Figure 2.1: A simple FDN structure,  $A$  is the feedback matrix. (Source: [15])

with a combination of a convolutional impulse response, used to model the onset, and a FDN for reproducing the reverb tail. This was necessary because, as it will be shown later, plate reverberation presents no early reflections, and a dispersive behaviour, characteristics which a FDN alone cannot achieve.

## 2.2 Convolution

Convolution reverberation essentially consists in modeling rooms, or other reverberation devices, as finite impulse response (FIR) filters, to be applied to the incoming signal [19, 20]. It is known that linear and time invariant systems can be completely characterized by their impulse responses (IRs)  $h(t)$ . In this kind of reverberation, the desired system impulse response is measured, through an impulse or a sine sweep, or calculated mathematically through computer simulations. Then, the incoming sound is convolved with the IR, to obtain the reverberated signal, as shown in equation (2.1), in the continuous domain.

$$y(t) = (x * h)(t) = \int_{-\infty}^{\infty} x(t - \tau)h(\tau)d\tau \quad (2.1)$$

Convolution reverberation is a widely used technique, as it allows to obtain very realistic and accurate reproductions of physical systems sounds, without

needing to previously perform time consuming and expensive simulations, provided that the IRs are correctly measured. In addition, computing an FIR can be done in real time, without any processing delay, making convolution apparently efficient; in practice though, this method presents many drawbacks. The first issue is computational load: for a 1 second long IR, sampled at 48 kHz, convolution requires to perform 48000 operations for each output sample, which doubles for stereo signals. This is easily achieved by modern computers, but can become quite challenging for embedded systems, especially if other operations need to be performed at the same time. Another problem linked to convolution is that, once the IR is measured, it is impossible to control the system parameters. In fact, an IR is a "photograph" of the current system state, and cannot be modified afterwards. In order to provide some control possibilities, the only solution is to measure several IRs with varying parameters, and then perform some kind of interpolation between them. The latter issue is not a big problem in the case of room modeling, where physical characteristics do not experience big changes, but it is an important limitation in the case of, for example, virtual analog modeling, where a high grade of control is usually requested. For this reason, convolution for virtual analog modeling is usually used in combination with other techniques which allow to provide more control, as seen in [18].

## 2.3 Physical Modeling

Physical modeling is a family of sound synthesis techniques which focus on the physics of the objects to be modeled. They consist in creating a mathematical model of the system at hand, and then discretise it with various numerical methods. In the context of room reverberation this means to determine the value of the sound pressure inside the acoustic space for each time instant. Physical modeling methods allow to obtain very accurate models, controllable in every detail, in fact, each physical parameter can be singularly adjusted. On the other hand though, they require hard and time consuming prior studies in order to formulate a precise mathematical model. In addition, these techniques are usually very computationally demanding, to the point that, sometimes, the simulation cannot be run in real time. This is particularly true in the case of reverbs: in fact, solving the 3-D wave equation for large acoustic spaces in real time goes beyond the capacities of modern personal computers. In this cases, it is possible to calculate a mathematical IR, to be convolved with the input signal.

Physical modeling for reverberation can be divided into two main groups [1]. The first one is *Geometrical Acoustics*: it consists in modeling sound as beams which propagate from a source in the surrounding space, and then to model all the possible paths and consequent walls reflections. The second group contains the *Wave-Based Methods*, which aim to numerically solve the wave equation. Since the first

family is not too suitable for virtual analog modeling, this paragraph will focus on the second one. In order to numerically simulate the wave equation, the domains of definition need to be discretised. One domain is always space, which defines the acoustic environment, the other one depends on the method: the Finite Element Method (FEM) operates on the frequency domain, whereas Finite-Difference Time-Domain (FDTD) methods on the time domain. In the context of reverberation, the latter methods are usually preferred because, by operating on time, they allow to directly obtain mathematical impulse responses, as seen in [21]. FDTD methods for numerically solving partial differential equations were already known before computers were born. In the context of room acoustic modeling, these techniques were used for the first time in the 90s [22]. In this work, Savioja et al. demonstrated the potentialities of wave-based techniques, which inherently include physical phenomena such as diffraction and interference. A more detailed description of FDTD methods will be provided in chapter 4. Digital Waveguides Meshes (DWGs) is a technique based on FDTD methods. Smith [23] was among the firsts to exploit this approach in the context of physical modeling, by developing simulations of several musical instruments using 1-D and 2-D interconnected digital waveguides structures. Nevertheless, DWGs can be easily extended to 3 dimensions, in order to model acoustic spaces [24, 25]. The principle of this technique is to perform a discretisation of the d'Alembert solution of the wave equation using bi-directional delay lines with commuted losses and phase inversions. A comparison between DWGs and more "classic" FDTD techniques has been done by Erkut and Karjalainen [26, 27]. The main difference which emerges is that DWGs perform a discretization of the system solution, whereas in classic FDTDs the partial differential equations are directly numerically calculated. This results in a higher efficiency of DWGs, which, however, are less flexible. In fact, since they are based on the lossless solution of the wave equation, any losses or nonlinearities need to be previously calculated and lumped at the extremes of the delay lines. On the other hand, in FDTD methods these are directly solved inside the equation.

### 2.3.1 Physical Modeling for Plate Reverberation Simulation

Given the accuracy and flexibility of physical modeling techniques, these have been widely used for modeling plate reverbs, in particular FDTD methods. In fact, contrary to other reverberation techniques such as convolution or delay networks, creating a mathematical model of the device allows to provide control on every single detail of it, and to directly model the widely appreciated sound characteristics such as dispersion and absence of early reflections. In addition, since the plate can be considered as 2-dimensional, solving the wave equation in real time is achievable, provided that some kind of optimization is performed. As dispersion is not so easily implementable with DWGs, physical models of plate reverbs usu-

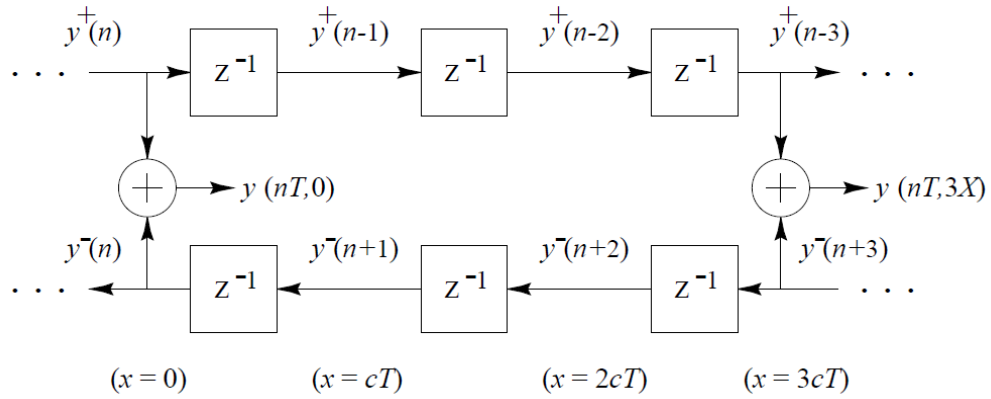


Figure 2.2: A 1-D digital waveguide (Source: [23])

ally employ more classic FDTD methods. First studies on the simulation of plate vibrations in the context of acoustics were performed by Chaigne et al. [28, 29]. In these works, classic FDTD methods are used to perform a simulation of a generic plate vibrations using the Kirchhoff-Love model for orthotropic plates; in addition, a thorough model for damping is developed, which takes into account thermoelasticity, viscosity and radiation. Later, a similar work was developed by Bilbao et al. [30], who implemented a simulation of a plate with physical parameters which matched the ones of the EMT 140, using the Kirchhoff model of plates and by directly discretising the wave equation using FDTD methods. This work differs from the ones by Chaigne et al. in the way damping is obtained. Here, a model usually used for strings is implemented, which involves two terms representing the frequency dependent and independent damping, with coefficients that are adjusted to match the desired sound. The Bilbao model makes use of a 2-dimensional Dirac delta for exciting the plate for modeling the punctual actuator, and free boundary conditions, thus ignoring the presence of the steel wires. Subsequently, Arcas published a work [31] in which he extended the solution proposed by Bilbao, including a more accurate model for damping, which will be extensively discussed in chapter 3. Arcas also dedicated his PhD studies to plate reverberation; in his thesis [2], he proposed to numerically solve the Kirchhoff model of the plate by using a modal approach, which will be illustrated in chapter 4. A similar modal method has been employed by Ducceschi and Webb [32], who developed a physical model of the EMT 140 plate reverb which can be run in real time inside a plugin. In this work, the use of a modal approach allows to run only the most perceptually relevant modes of the plate, thus reducing the computational power needed for running the algorithm. Here, damping is implemented by manually setting the  $T_{60}$  for eight different frequency bands, a method that provides to the user more control over the output sound. Lately, Willemsen et al. [33] employed the same modal

approach with modes reduction used by Ducceschi and Webb for implementing a real time plugin. Here though, damping is calculated by using mathematical models similar to the ones saw in Arcas work, except for the damping induced by the porous medium, which is not taken into account.

## 2.4 Neural Networks

Neural networks are machine learning techniques fastly growing nowadays. In the context of reverbs, these algorithms have been more extensively used for dereverberation; however, in recent years, many black-box models of audio effects have been proposed by using deep learning architectures [34]. Lately, a model for plate reverberation which makes use of Deep Neural Networks (DNNs) have been proposed by Martínez Ramírez et al. [35]. Listening tests reported in the study showed that the model is capable of reproducing accurate sounds, however, the black box modeling nature of the algorithm makes modeling parameters control quite challenging. Nevertheless, investigation of machine learning solutions for virtual analog plate reverberation is beyond the scope of this project.

## 2.5 Commercial Plugins

Over the years, many different audio plugins which emulate plate reverberation were introduced on the market; this section reports the most relevant ones. Since these are commercial solutions, knowing the modeling technique which runs under the hood is not always possible, therefore, it will be mentioned only when available.

### 2.5.1 Universal Audio EMT 140 Classic Plate Reverberator

One of the first commercial plate reverb plugins, the Universal Audio EMT 140 Classic Plate Reverberator [36] came out in 2010, and provides a model of the EMT 140 plate reverb. The company does not give information on the technology used. The only available plate controls are plate type and reverberation time in seconds.



Figure 2.3: EMT 140 Classic Plate Reverberator. (Source: [36])

### 2.5.2 IK Multimedia CSR Plate Reverb

Presented in 2011 as a part of the T-Racks suite, the CSR Plate Reverb [37] provides a model of a generic plate reverb. The plugin presents two control modes: *easy* and *advanced*. In both modes, many control possibilities are present, allowing for fine tuning of the plate. In easy mode, the plate related controls are: diffusion, reverb time (in seconds), low time, high frequency cutoff, high frequency damping. In advanced mode these are, time related: reverb time, low time, crossover, high frequency cutoff, high frequency damping pre delay. Reverb related: size, diffusion, buildup disperse modulation. Color related: low cutoff frequency, low cutoff gain, high cutoff frequency, high cutoff gain. Reflections related: time left, level left, time right, level right. Echo related: time left, feed left, time right, feed right. The company does not provide details on the implementation.



Figure 2.4: CSR Plate Reverb. (Source: [37])

### 2.5.3 Waves Abbey Road Reverb Plate

Presented in 2016 by Waves, the Abbey Road Reverb Plate [38] models the plate reverb from the Abbey Road studios in London. For this reason, the controls are quite limited. For what concerns the plate, it is possible to change the plate kind and the damper amount, while the transducer and accelerometers locations remain fixed. The company does not provide information on the algorithm nature.

### 2.5.4 Arturia Rev PLATE-140

The Rev PLATE-140 [39] was launched in 2019 by Arturia. The company does not provide details on the implementation, however, they state that the plugin includes an accurate model of the vacuum tube preamp, meaning that some virtual analog techniques have been employed. The fact that the plate width is also controllable suggests that some modeling methods other than convolution have been used. Other controls include changing the plate type and controlling the preamp.



Figure 2.5: Abbey Road Reverb Plate.



Figure 2.6: Rev PLATE-140 (Source: [39])

### 2.5.5 Valhalla Plate

Launched in 2015 by ValhallaDSP, Valhalla Plate [40] is the first plugin presented specifically as a virtual analog model. This characteristic got consumers really interested in the product [41], as the model allowed very fine control, to the point that it was possible to obtain almost unreal sounds. From the plate standpoint, the plugin allows to control the size, width and material of the plate, along with the decay rate (up to 30 seconds).

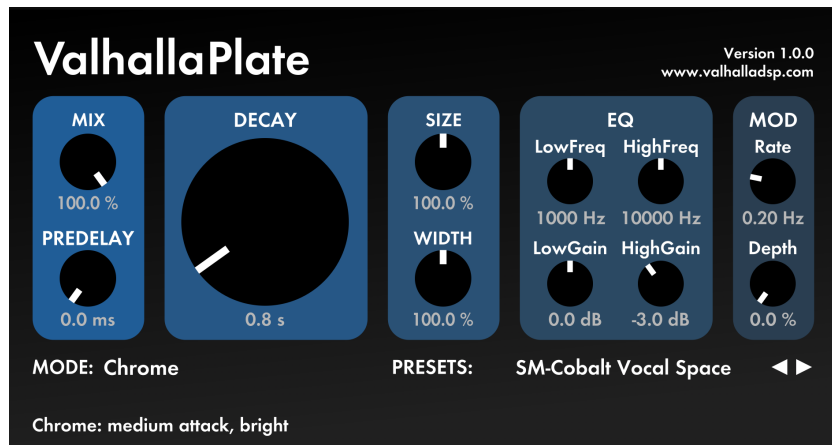


Figure 2.7: Valhalla Plate. (Source: [40])

### 2.5.6 Physical Audio PA1 Dynamic Plate Reverb

The PA1 Dynamic Plate Reverb [42] is the first plugin presented by the Physical Audio company. It was launched in 2016 and it is based on the work by Ducceschi and Webb previously mentioned [32], making this a virtual analog physical model. As said above, here damping is implemented by setting the decay rate for eight frequency bands, allowing for a high level of control over the plate. The other plate-related controllable parameters are: plate material, plate size, stereo pickups positions, plate tension, input moving.

### 2.5.7 UVI Plate

UVI Plate [43] was launched in 2018 by the French company UVI. It is presented as a physical model, making this another virtual analog simulation. Among many nice features, this plugin presents a physically based model of damping, which takes into account also the damping induced by the porous damper, with a controllable decay rate. Nevertheless, no study has been published yet by the company, therefore an evaluation of the damping model employed is not possible. This plugin allows to control: plate area, aspect, anisotropy (in percentage), tension,



Figure 2.8: PA1 Dynamic Plate Reverb. (Source: [42])

modulation and material. The decay rate can be controlled with a single global parameter or with a frequency bands scheme, as seen in the PA1. In addition, it is possible to set the amount of thermoelastic and viscous damping desired. The possibility to control anisotropy suggests that some enhancements may have been added to the classic Kirchhoff model.

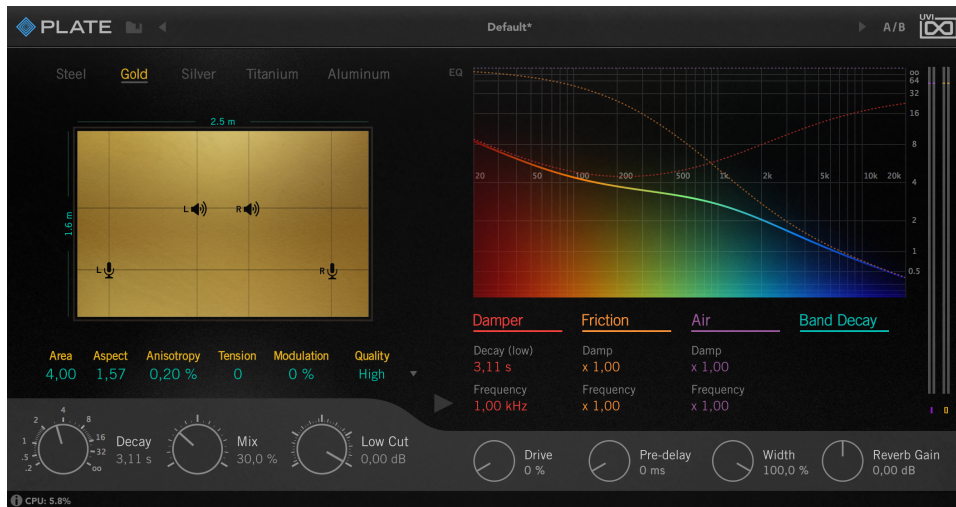


Figure 2.9: UVI Plate. (Source: [43])

## 2.6 Project Goal

In this work, a physical model of a EMT 140 plate reverb is proposed, which makes use of a modal approach and a FDTD method, and is implemented with the MAT-

LAB programming language. A physical modeling approach was chosen as it allows to provide control on every single detail of the plate sound. Since, as it was previously showed, this method is quite computationally expensive, an optimization technique was also implemented, based on linear least squares. The work starts by developing a model previously proposed by Ducceschi and Webb [32], implementing it with a Finite Difference Scheme which exactly solves the harmonic oscillator equation. Then, an implementation of a physical damping is performed, based on previous studies, which includes the dependency on the distance of the damper panel from the plate, as it happens in the real device. Lastly, an optimization technique is proposed, based on previous studies on room reverberation, which allows for a reduction of the number of modes to be calculated in parallel, and, as a consequence, of the computational power needed. This manuscript is organized as follows: in chapter 3, the mathematical model of the plate is derived, including the damping model and the modal decomposition. In chapter 4, the equations are discretised and considerations over the accuracy of the discrete scheme are made. Chapter 5 focuses on the optimisation technique. In chapter 6 results are provided and, finally, chapter 7 concludes the paper.

## Chapter 3

# Plate Model in the Continuous Domain

In this work, a virtual analog model of the EMT 140 plate reverb based on a physical model is built. In order to do this, the first thing to do is to develop a mathematical model which can describe the system. It was chosen to use a modal approach similar to the one proposed by Arcas, and utilised also by Ducceschi and Webb, described in chapter 2. In fact, it proved to achieve accurate reproductions of the plate sound, while being more easily optimisable, contrary to the more "direct" approach utilised by Bilbao et al. [30]. This chapter describes the plate model in the continuous domain. First, the Kirchhoff-Love model of the plate is described, then details on the modal decomposition are provided, and finally the damping model implemented is illustrated.

### 3.1 Kirchhoff-Love Model

The Kirchhoff-Love model is a linear model which describes vibration of plates. A plate is an object which extends in two spatial dimensions:  $x$  and  $y$ , with axial lengths  $L_x$ ,  $L_y$ , and has a finite thickness  $H$ . This model is valid under the assumption that  $H \ll L_x, L_y$ . The equation governing the plate is given by [44]:

$$\rho H \ddot{u}(x, y, t) = -D \nabla^4 u(x, y, t) + f(x, y, t) \quad (3.1)$$

It is a partial differential equation (PDE) in two spatial dimensions plus time. Here,  $u$  represents the local vertical (along the  $z$  axis) displacement of the plate at the instant  $t$ , and the domains of definition for  $x$  and  $y$  are given by the plate dimensions, respectively:  $[0, L_x]$ ,  $[0, L_y]$ . The constant  $\rho$  is the plate material density,  $[\rho] = [kg/m^3]$ ,  $f$  is the input forcing function,  $H$  is the plate thickness and  $\nabla^4$  is a

squared Laplacian, or biharmonic operator, defined as:

$$\frac{\partial^4}{\partial x^4} + 2\frac{\partial^4}{\partial x^2\partial y^2} + \frac{\partial^4}{\partial y^4} \quad (3.2)$$

The constant  $D$ , sometimes referred to as the flexural rigidity, depends on the plate physical characteristics:

$$D = \frac{EH^3}{12(1-\nu^2)} \quad (3.3)$$

where  $E$  is the plate Young's modulus and  $\nu$  is the Poisson's ratio. If one divides the right member of the equation by the constants present in the left hand side he obtains a constant:

$$\kappa^2 = \frac{D}{\rho H} = \frac{EH^2}{12\rho(1-\nu^2)} \quad (3.4)$$

which is usually defined as the *stiffness parameter*. Therefore, the plate equation becomes:

$$\ddot{u}(x, y, t) = -\kappa^2 \nabla^4 u(x, y, t) + \frac{f(x, y, t)}{\rho H} \quad (3.5)$$

In this form, the governing PDE can be seen as an extension in two dimensions of the linear bar wave equation [45]. As in the latter case, the presence of fourth derivatives introduces a dispersive behaviour, which will be further investigated in the next paragraph.

### 3.2 Dispersion Relation and Wave Propagation

Information on the frequency behaviour of equation (3.5) may be obtained by inserting a test solution of the form:  $u(\mathbf{x}, t) = e^{st+i\boldsymbol{\beta}\mathbf{x}}$ , where  $s = \sigma + i\omega$  is a complex frequency and  $\boldsymbol{\beta} = \beta_x, \beta_y \in \mathbb{R}^2$  are the wavenumbers, into the unforced plate equation [45]. Doing this yields:

$$s^2 = -\kappa^2 \boldsymbol{\beta}^4 \quad (3.6)$$

Since the equation is lossless, it is possible to set  $\sigma = 0$ , thus obtaining the dispersion relation:

$$\omega^2 = \kappa^2 \boldsymbol{\beta}^4 \quad (3.7)$$

Consequently, phase and group velocities can be obtained:

$$c_{ph}(\boldsymbol{\beta}) = \kappa|\boldsymbol{\beta}| \quad c_{gr}(\boldsymbol{\beta}) = 2\kappa|\boldsymbol{\beta}| \quad (3.8)$$

By using (3.7), it is also possible to express the relations above in terms of the frequency  $\omega$ :

$$c_{ph}(\omega) = \sqrt{\kappa\omega} \quad c_{gr}(\omega) = 2\sqrt{\kappa\omega} \quad (3.9)$$

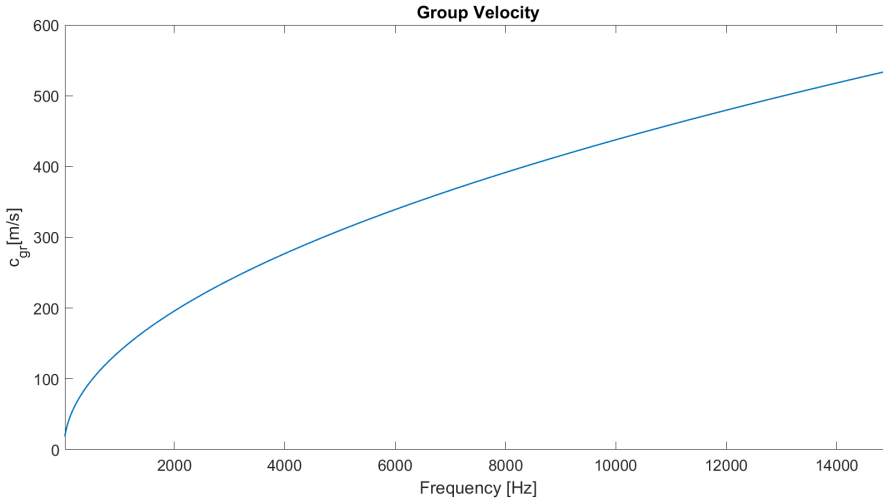


**Figure 3.1:** Group velocity as a function of frequency.

Looking at equations (3.9), it is clear that both velocities depend on the wavenumber: this means that higher frequencies travel faster than lower ones, as shown in Figure 3.1. This is in sharp contrast to what happens in room reverberation. Air is a non-dispersive medium, therefore, the reflected waves are not distorted, this allows to easily recognize the direct sound and the echoes in the early part of the reverberation (this is particularly noticeable in large spaces, for example in the "echo" phenomenon). On the contrary, the dispersive behaviour of the plate distorts the input signal, making it impossible to reconstruct the waveform at the output points. In the specific case of the EMT 140, for what concerns the audio band, the group velocity is between 20 and 628 m/s. Considering the position of only one of the accelerometers, this means that the first wave arrives after 1 ms, while the last one after 30.1 ms [31]. Since the human hearing is able to perceive this delay, dispersion is probably one of the features that make the EMT 140 sound so iconic.

### 3.3 Loss and Tension

The classic Kirchhoff model can be extended to take into account damping and an applied tension, thus obtaining a general model of a stiff membrane [46]:

$$\rho H \ddot{u}(x, y, t) = T_0 \nabla^2 u(x, y, t) - D \nabla^4 u(x, y, t) - 2\sigma \rho H \dot{u}(x, y, t) + f(x, y, t) \quad (3.10)$$

where  $T_0$  is the tension and  $\sigma$  a damping parameter. In this form, the damping factor represents a total, frequency independent, loss. However, when the model will be decomposed in a modal form, it will be possible to set it in a frequency

dependent manner. The coefficient  $\sigma$  is linked to the  $T_{60}$  by the relation:

$$\sigma = 6 \frac{\ln(10)}{T_{60}} \quad (3.11)$$

### 3.4 Damping

Damping determines the sound decay over time. It is a natural phenomenon, which occurs due to the attenuation of acoustic waves during the course of their path, as the vibrational energy is converted into other kinds of energy. In plate reverberation sounds are naturally damped by the internal device structure; in addition, a porous panel can be moved near the plate to provide some control over the decay time. According to Arcas and Chaigne [47], there are four main sources of loss: thermoelasticity, radiation in the free field, radiation into the porous medium and energy losses where the plate is attached to the structure. The latter is the most difficult to model, and a correct implementation would need to perform measurements on a real physical device: for this reason it will be neglected.

#### 3.4.1 Thermoelastic Damping

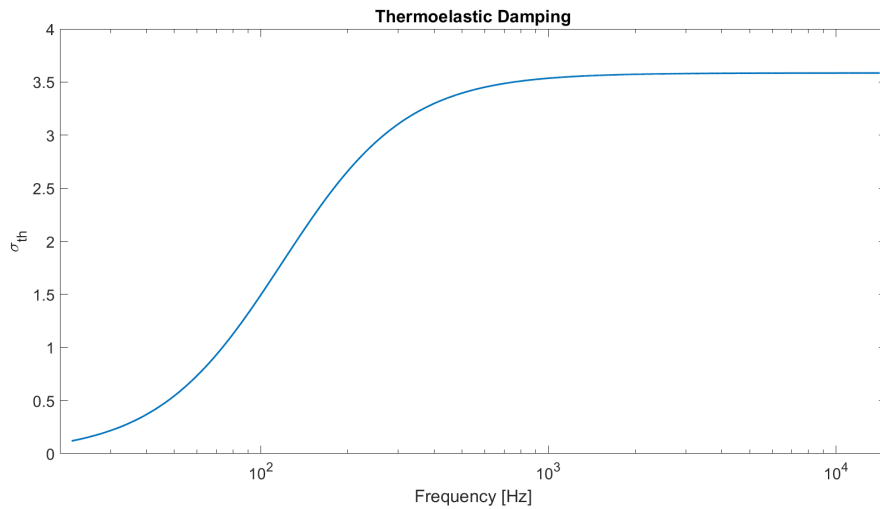


**Figure 3.2:** Thermoelastic Damping for the EMT 140 plate made of Carbon Steel SAE 1010.

Thermoelastic damping is particularly present in materials such as metals, which present a high thermal conductivity, and it is due to the conversion of elastic waves into heat. This phenomenon causes different frequencies to decay at different rates. A relation which links thermoelastic damping to the loss coefficients  $\sigma$  is given in [47]:

$$\sigma(\omega) = \frac{\omega^2 R_1 C_1}{2(\omega^2 H^2 + C_1^2 / H^2)} \quad (3.12)$$

which, for  $\omega \rightarrow \infty$  tends to:

$$\sigma_\infty = \frac{R_1 C_1}{2H^2} \quad (3.13)$$

Here,  $R_1$  and  $C_1$  are coefficients which depend on the plate material characteristics. Figure 3.2 reports the values of the damping coefficients  $\sigma$  in relation to the frequency, relative to the thermoelastic damping. The physical parameters are the ones for the Carbon Steel SAE 1010, namely:

$$R_1 = 9.664 \times 10^{-3} \quad C_1 = 0.1855 \times 10^{-3}$$

It is possible to prove that the value of  $\sigma$  reaches the 95% of  $\sigma_\infty$  at around 500 Hz, making the damping almost constant for higher frequencies.

### 3.4.2 Radiation Damping

Radiation damping occurs because of the conversion of vibrational energy into acoustic energy: it is the reason why we can hear the plate vibrating. This kind of loss is closely linked to the radiation efficiency, which is the ratio between the sound power radiated from a source and that of a piston of the same size, moving with the same average velocity [48]. For an infinite plate, radiation efficiency is given by [47]:

$$\alpha = \frac{W_{rad}}{\rho_a c_a S \langle \bar{v}^2 \rangle} \quad (3.14)$$

where,  $W_{rad}$  is the total sound power radiated from the structure,  $\rho_a$ ,  $c_a$  are, respectively, the density of air and sound speed in air. and  $\langle \bar{v}^2 \rangle$  is the spatial average of the mean squared value of the transverse velocity of the structure. Another important parameter concerning radiation damping is the concept of critical frequency  $f_c$ : it is the frequency at which the speed of bending waves in the structure becomes equal to the one of acoustic waves on air [49]. Therefore, for frequencies above  $f_c$  the structure radiates efficiently, while below the radiated power is low. A formula for the plate critical frequency is given by Arcas and Chaigne [47], together with a model of radiation damping for the EMT 140. For an isotropic plate,  $f_c$  is given by:

$$f_c = \frac{c_a^2}{2\pi\kappa} \quad (3.15)$$

For the EMT 140 the critical frequency results:  $f_c \approx 25$  kHz, thus, radiation is poor in the audio band. This is indeed an important characteristics, in fact, it means that, in the audible range, the rate of conversion of vibrational waves into sound

is low, and thus signal loss is poor. The relation between radiation efficiency and damping is given by:

$$\sigma = \frac{\rho_a c_a}{\rho H} \alpha \quad (3.16)$$

Arcas and Chaigne retrieve a formula for radiation damping starting with a model by Maidnaik [50], which takes the form:

$$\sigma = \frac{1}{4\pi^2} \frac{\rho_a c_a}{\rho H} \frac{2(L_x + L_y)}{L_x L_y} \frac{c_a}{f_c} g(\psi) \quad (3.17)$$

With:

$$g(\psi) = \frac{(1 - \psi^2) \ln[(1 + \psi)(1 - \psi)] + 2\psi}{(1 - \psi^2)^{3/2}} \quad (3.18)$$

and

$$\psi = \sqrt{f/f_c} \quad (3.19)$$

The values of the damping coefficients relative to radiation damping are illustrated in Figure 3.3. As expected, damping increases sharply when getting closer to the critical frequency.

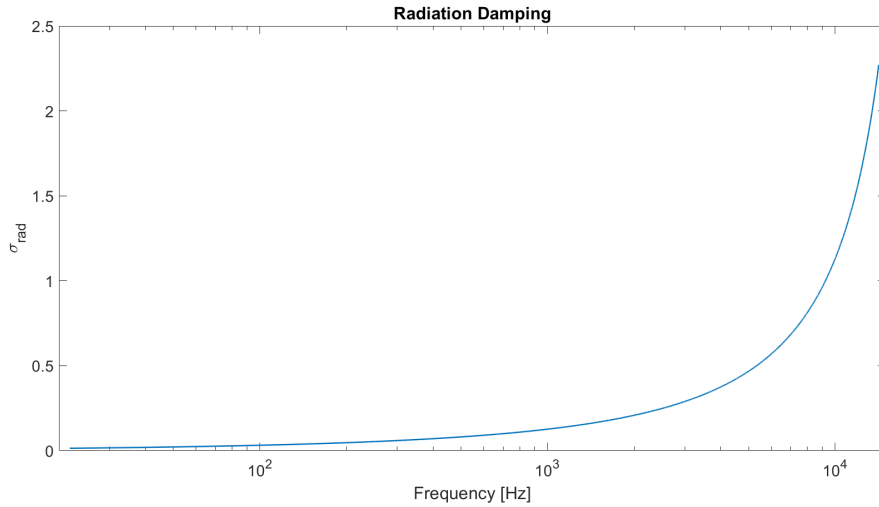


Figure 3.3: Radiation Damping for the EMT 140 plate made of Carbon Steel SAE 1010.

### 3.4.3 Damping induced by a Porous Medium

As previously mentioned, the reverberation time in the EMT 140 can be controlled by moving a panel made of a porous material closer or further from the vibrating plate. This method employs the impedance discontinuity created by a medium different than air in the nearfield of the plate to increase the radiated power, thus

increasing loss. Cummings et al. [51] studied this kind of sound damping in the context of sound insulation for aircraft fuselages, in which a porous material, typically a thermal insulator, is placed between two (outer and inner) metallic panels. In his work, Cummings provided an empirical model for describing the effects on sound of a layer of porous material placed a distance away from a vibrating, simply supported plate. The absorbent is here considered to be of semi-infinite dimensions, and an equivalent fluid model is used to describe it, with parameters obtained through empirical measurements. The acoustic impedance  $Z$  of the porous material depends on the sound frequency and is given by:

$$\frac{Z(f)}{\rho_a c_a} = 1 + c_1 \zeta^{c_2} - i c_3 \zeta^{c_4} \quad (3.20)$$

while the propagation coefficient:

$$\frac{\Gamma(f)}{k_a} = c_5 \zeta^{c_6} + i(1 + c_7 \zeta^{c_8}) \quad (3.21)$$

where

$$\zeta = \rho f / R \quad (3.22)$$

Here,  $\rho_a$ ,  $c_a$  and  $k_a$  are the density of air, sound speed and wavenumber in air,  $f$  is the frequency in Hz and  $R$  is the material flow resistivity, measured in rayl/m (MKS). Finally,  $c_{1-8}$  are coefficients measured empirically. Equivalent fluid density  $\rho$  of the porous material and sound speed  $c$  in it can be retrieved with the relations:

$$c = \frac{i\omega}{\Gamma}, \quad \rho = \frac{Z\Gamma}{i\omega} \quad (3.23)$$

Later, Craik and Allard [52] revised Cummings work and proposed an analytical model for describing the radiation of a vibration plate into a porous medium. In this paper, Craik defines two mathematical solutions to the problem: one takes into account the absorbent panel dimensions, and the other considers it to be infinite. Then, he shows that the two solutions yield identical results, implying that the simpler, infinite case can be equivalently utilised for tackling the problem. Craik's model considers the porous panel to be at infinitesimal distance from the metallic plate and does not provide information on the dependency on the gap size, therefore it cannot be employed to model the EMT 140 damper. However, the paper provides an alternative equivalent fluid model for the absorbent, based on previous studies. Material density is given by:

$$\rho = 1.2 + \sqrt{\frac{-0.0364}{\zeta^2} - \frac{i0.1144}{\zeta}} \quad (3.24)$$

While the sound speed in the medium:

$$c = \sqrt{\frac{101320}{\rho} \frac{i29.64 + \sqrt{2.82/\zeta^2 + i21.17/\zeta}}{i29.64 + \sqrt{2.82/\zeta^2 + i24.9/\zeta}}} \quad (3.25)$$

Where:

$$\xi = \rho_a f / R \quad (3.26)$$

And  $R$  is still the flow resistivity in rayl/m (MKS).

After Craik's publication, Cummings extended the analytical model, providing a relation which includes the dependency on the gap size between the plate and the absorbent [53]. This model describes the phenomenon in terms of the radiation efficiency, which is given by:

$$\alpha = k_a \Re[F(\omega)] \quad (3.27)$$

Here,  $k_a$  is the wavenumber in air, while  $F(\omega)$  is:

$$F(\omega) = \frac{1 + \gamma}{k_c(1 - \gamma)} \quad (3.28)$$

Where,  $k_c = \sqrt{k_a^2 - k_b^2}$  and  $k_b = \sqrt{\omega(m/D)^{1/4}}$  is the wavenumber in the plate, while  $m$  is the mass per unit area of the plate. Finally,  $\gamma$  is given by:

$$\gamma = \frac{-\exp(-2ik_c d)[1 - \exp(-2ik_d h)]}{\Theta - \exp(2ik_d h)\Theta} \quad (3.29)$$

and

$$\Theta = \frac{\tau + 1}{\tau - 1}, \quad \tau = \frac{k_d \rho_a}{k_c \rho} \quad (3.30)$$

Here,  $h$  is the porous material thickness,  $d$  is the distance between the material and the plate, and  $k_d = \sqrt{k^2 - k_b^2}$ , where  $k = \omega/c$  is the wavenumber in the absorbent material. In this work, Cummings also provides the relation which links radiation efficiency to the  $T_{60}$ :

$$\alpha = 13.82 \frac{m}{\rho_a c_a T_{60}} \quad (3.31)$$

The damping coefficients can then be obtained by using equation 3.11.

In [47], Arcas and Chaigne provide a graph showing the damping induced by a porous medium, obtained following Cummings studies. The graph is reported in Figure 3.4. Nevertheless, the model used for the porous material differs from the two showed above. In this work, we tried to set different porous material characteristics in both Craik and Cummings models, in order to visually match the results reported by Arcas and Chaigne. Figure 3.5 shows the damping factors obtained by using the equivalent fluid model reported by Craik for the porous material. In this case, the flow resistivity was set to  $R = 20000$  rayl/m, in order to obtain comparable peak values. The distance was set to 11 mm (blu) and 17.2 mm (orange) to match the values provided by Arcas, and the thickness of the porous panel was set to  $h = 0.1$  m. In the case  $d = 11$  mm the peak value is similar to the one showed in Figure 3.4, while for  $d = 17.2$  mm it is completely

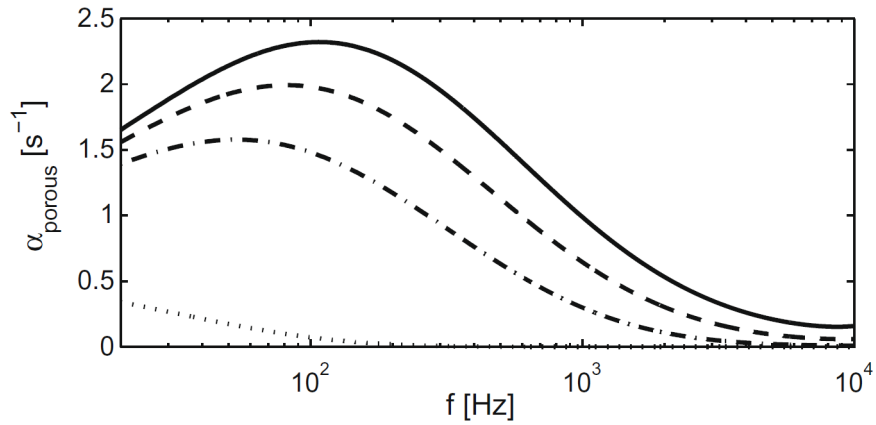


**Figure 3.4:** "Damping factor induced by the porous plate computed with Cummings model for different distances between the plates:  $d = 65.8$  mm (dotted);  $17.3$  mm (dash-dotted),  $13.2$  mm (dashed);  $11.0$  mm (solid)." (Source: [47])

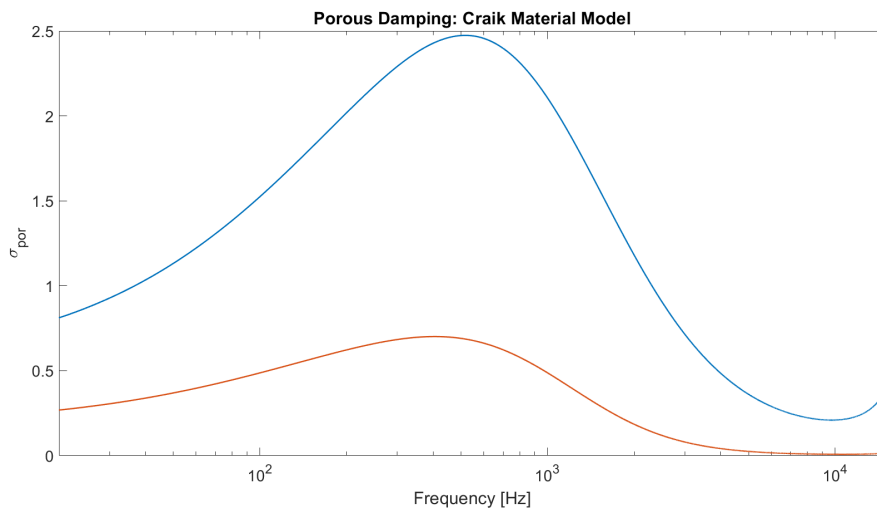


**Figure 3.5:** Radiation into a porous medium obtained with the model of the absorbed material given by Craik, with a flow resistivity of  $R = 20000$  rayl/m, for different distances of the panel from the plate:  $d = 11$ mm (blue),  $d = 13.2$ mm (orange).

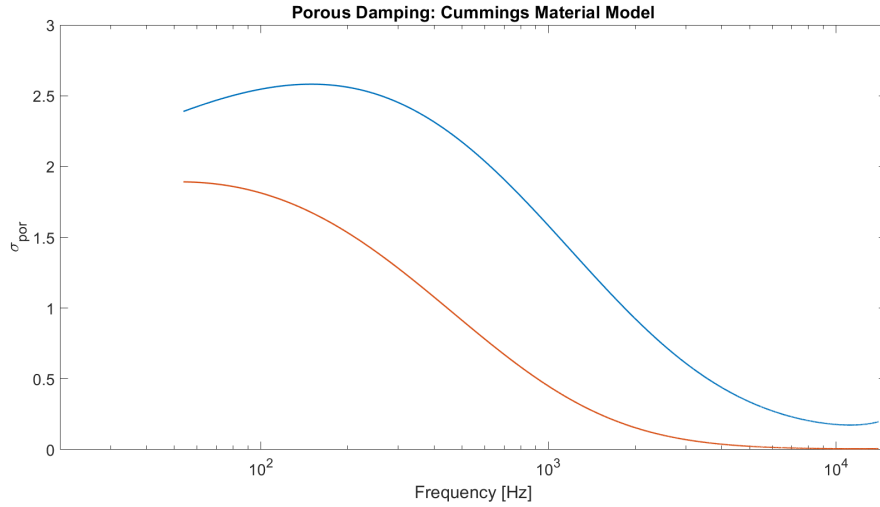


**Figure 3.6:** Radiation into a porous medium obtained with the model of the absorbed material given by Cummings, with a flow resistivity of  $R = 70000$  rayl/m, for different distances of the panel from the plate:  $d = 11$ mm (blue),  $d = 13.2$ mm (orange).

underestimated. In both cases, the curves trend does not match the ones provided by Arcas. In Figure 3.6 are illustrated the damping factors obtained by using the model reported by Cummings for the absorbent. The panel distances and thickness are the same used with the Craik model, however, this time it was necessary to set the flow resistivity to  $R = 70000$  rayls/m for matching the peak values. In this case, the curves shapes have a trend which looks more similar to the one in Figure 3.4, however, a numerical error makes it impossible to calculate the damping factors below 50 Hz. Since both models are affected by some issues, it was decided to keep them inside the algorithm, letting the user choosing which one to use.

### 3.5 Modal Analysis

In [30], Bilbao et al. presented a physical model of the EMT 140 which works by directly discretising the plate equation (3.10) with a space-time grid and simulating it with a finite difference scheme. This approach allows for a fast implementation of a physical model, while still providing control over many parameters; however, it presents some issues. In particular, the integration of frequency damping is not so straightforward, and the model is very computationally demanding. Another method is to use modal analysis to decompose the Kirchhoff equation into its normal modes of vibration. In this section, the modal decomposition of the plate equation will be detailed, following the work by Ducceschi and Webb [32], this will be the basis for the simulation of the system.

Modal analysis consists in exploring the circumstances in which the motion

of an object is synchronous: under these conditions, the profile of the vibrating object does not change, only amplitude does. From a mathematical standpoint, this means that the problem is *separable* in space and time, therefore the solution to the problem can be expressed as:

$$u(\mathbf{x}, t) = Y(\mathbf{x})F(t) \quad (3.32)$$

The expansion theorem [54] ensures that, in order to start tackling the problem, it is possible to consider the equation without loss and forcing. Therefore one can start by trying to solve:

$$\rho H \ddot{u}(x, y, t) = T_0 \nabla^2 u(x, y, t) - D \nabla^4 u(x, y, t) \quad (3.33)$$

In this case, it can be assumed that the solution  $u(x, y, t)$  takes the separable form [55]:

$$u(x, y, t) = \sum_{m_1=1}^{M_1} \sum_{m_2=1}^{M_2} \Phi_{m_1, m_2}(x, y) A_{m_1, m_2} \sin(\omega_{m_1, m_2} t + \phi_{m_1, m_2}) \quad (3.34)$$

Where  $M_1$  and  $M_2$  are supposed to be infinite, but will be limited in practice. The modal amplitudes  $A_{m_1, m_2}$  and phases  $\phi_{m_1, m_2}$  can be determined from the boundary and initial conditions. By inserting (3.34) into (3.33) one obtains:

$$\omega_{m_1, m_2}^2 \phi_{m_1, m_2}(x, y) = \frac{D}{\rho H} \nabla^4 \phi_{m_1, m_2}(x, y) - \frac{T_0}{\rho H} \nabla^2 \phi_{m_1, m_2}(x, y) \quad (3.35)$$

Which is a *differential eigenvalue problem*. Solving it, after having set boundary conditions, means finding the roots  $\omega_{m_1, m_2}$  of the characteristic polynomial, which are known as *eigenfrequencies*, for each of which there will be an associated eigenfunction  $\Phi_{m_1, m_2}(x, y)$ . Together, these are called normal modes of vibration, and it can be proved that they form an orthonormal set over the  $L_2$  space [54]. Since the number of eigenfrequencies is typically infinite, it is possible to say that there exists an infinite number of ways in which the motion of a system is synchronous.

Once obtained the form of the eigenvalue problem, it is time to insert back loss and forcing. In this case the solution form (3.34) is not valid anymore because the time component does not oscillate in a sinusoidal way, therefore it is possible to write the time component in a more generic way:

$$u(x, y, t) = \sum_{m_1=1}^{M_1} \sum_{m_2=1}^{M_2} \Phi_{m_1, m_2}(x, y) q_{m_1, m_2}(t) \quad (3.36)$$

One can then insert the solution above into equation 3.10, multiply by another random solution  $\Phi(x, y)_{m'_1, m'_2}$  and take the inner product. Considering the orthonormality of the modes it is obtained:

$$\ddot{q}_{m_1, m_2}(t) + \omega_{m_1, m_2}^2 q_{m_1, m_2}(t) + 2\sigma_{m_1, m_2} \dot{q}_{m_1, m_2}(t) - \frac{\Phi_{m_1, m_2}(x_p, y_p)}{\rho H} P(t) = 0 \quad (3.37)$$

For more information refer to: [54, 55]. What obtained here is a system of damped, forced uncoupled oscillators, which completely describes the system. Also, it appears clear how the damping coefficients  $\sigma_{m_1, m_2}$  can now be set singularly for each mode of vibration, making it possible to use the loss coefficients in the form obtained in the previous section. The modal decomposition allows to solve the complex PDE in equation (3.10) by only computing several oscillators in parallel. In addition, it makes it possible to discard the unnecessary modes, in order to save computational power. Doing this, of course, requires to know the form of the natural modes and the eigenfrequencies, which can be calculated by setting the boundary conditions. Being kept suspended by steel wires at the corners, the EMT 140 can be considered as freely vibrating. However, it is not so straightforward to obtain an analytical solution for the modes of a plate with free boundaries and numerical methods would be needed in order to calculate them. Nevertheless, things are different if considering simply supported boundaries [44], namely:

$$\begin{aligned} u(0, y) = \nabla^2 u(0, y) = u(x, 0) = \nabla^2 u(x, 0) = 0 \\ u(L_x, y) = \nabla^2 u(L_x, y) = u(x, L_y) = \nabla^2 u(x, L_y) = 0 \end{aligned} \quad (3.38)$$

Under these conditions, the normal modes of vibration take the form [32]:

$$\Phi_{m_1, m_2}(x, y) = \sqrt{\frac{4}{L_x L_y}} \sin \frac{m_1 \pi x}{L_x} \sin \frac{m_2 \pi y}{L_y} \quad (3.39)$$

Where  $L_x, L_y$  are the dimensions of the plate. The corresponding eigenfrequencies are:

$$\omega_{m_1, m_2} = \sqrt{\frac{T_0}{\rho H} \left( \frac{m_1^2 \pi^2}{L_x^2} + \frac{m_2^2 \pi^2}{L_y^2} \right) + \frac{D}{\rho H} \left( \frac{m_1^2 \pi^2}{L_x^2} + \frac{m_2^2 \pi^2}{L_y^2} \right)} \quad (3.40)$$

The current displacement at the desired output point  $(x_o, y_o)$  can therefore be obtained by computing the value of the modes oscillators at time  $t$ , and then projecting with the correct modes:

$$u(x_o, y_o, t) = \sum_{m_1=1}^{M_1} \sum_{m_2=1}^{M_2} q_{m_1, m_2}(t) \Phi_{m_1, m_2}(x_o, y_o) \quad (3.41)$$

A finite value for  $M_1$  and  $M_2$  will be introduced in the next chapter with the discretisation of the model.

## Chapter 4

# Discrete Simulation

In the previous chapter, a complete mathematical description of the plate in the continuous domain was obtained. Here, it will be described how the model was simulated with the use of a FDTD method, and the physical model algorithm will be presented. First, a brief discussion on finite difference schemes synthesis will be provided, which will be useful for describing the discretisation of the mathematical equations. Then, the oscillator model used will be presented, along with accuracy considerations. Finally, details on the optimization method used will be provided.

### 4.1 Finite Difference Schemes Synthesis

Finite difference schemes is a modeling technique based on FDTD methods. Essentially, it consists in discretising the domains of definition with finite sampling steps, thus creating a space-time grid. As previously mentioned, Bilbao et al. [30] used this method for creating a physical model of the EMT 140. In their work, equation (3.10) (with an added term for frequency dependent damping) was simulated by using a 3-dimensional grid, which allowed to obtain a direct approximation of the system solution  $u(x, y, t)$  in the form  $u_{l,m}^n$  where  $l, m$  are the spatial sampling steps defining the grid point, and  $n$  indicates the time sample.

In the present work, a change of coordinate system was performed, in order to decompose the full plate equation into a series of modes, which are nothing but uncoupled damped harmonic oscillators. Looking at equation (3.37) (ignoring the input component), it can be noticed how the modal description is independent from the space coordinates; indeed, these are not present in the relation for the eigenfrequencies obtained in (3.40) either. This means that the oscillators configuration is valid for each spatial point, and that the projection on the desired spatial coordinates can be simply obtained with a multiplication by the correspondent modes. For this reason, the only physical quantity which needs to be discretised is time. In order to do this, it is first necessary to set a sampling step  $k$ , which for

audio applications is usually linked to the sampling frequency  $f_s$  by:

$$f_s = 1/k \quad (4.1)$$

Therefore, the time component is discretised in the form:  $t = nk$ , where  $n = 0, 1, 2, \dots$  is a positive integer. This allows to approximate a time-dependent function  $q(t)$  with the discrete series:  $q^n$ .

It is now possible to define the *shift operators*:

$$e_{t+}q^n = q^{n+1} \quad e_{t-}q^n = q^{n-1} \quad (4.2)$$

Which are the basis for formulating more complex operators, in particular different approximations of the first order derivative:

$$\delta_{t+} := \frac{1}{k}(e_{t+} - 1) \approx \frac{\partial}{\partial t} \quad \delta_{t-} := \frac{1}{k}(1 - e_{t-}) \approx \frac{\partial}{\partial t} \quad \delta_t := \frac{1}{2k}(e_{t+} - e_{t-}) \approx \frac{\partial}{\partial t} \quad (4.3)$$

These are the *backward*, *forward* and *center* difference approximation respectively. If applied to the series  $q^n$  the difference operators yield:

$$\delta_{t+}q^n = \frac{q^{n+1} - q^n}{k} \quad (4.4)$$

$$\delta_{t-}q^n = \frac{q^n - q^{n-1}}{k} \quad (4.5)$$

$$\delta_t.q^n = \frac{q^{n+1} - q^{n-1}}{2k} \quad (4.6)$$

which are essentially different versions of finite difference quotient. The operators above can be then combined for obtaining higher order derivatives approximations, for example the second order derivative can be approximated by:

$$\delta_{tt}q^n := \delta_{t+}\delta_{t-}q^n = \frac{q^{n+1} - 2q^n + q^{n-1}}{k^2} \quad (4.7)$$

By using the Taylor expansion it is possible to calculate the accuracy of the difference operators. If one applies the operator (4.4) to the continuous function  $q(t)$  and expands in Taylor series obtains:

$$\delta_{t+}q(t) = \frac{q(t+k) - q(t)}{k} = \frac{1}{k}[k\dot{q}(t) + \frac{k^2}{2!}\ddot{q}(t) + \dots] = \dot{q}(t) + \mathcal{O}(k) \quad (4.8)$$

Therefore, the forward operator approximates the first derivative with an accuracy which scales with the first power of  $k$ , indeed, it is said to be first order accurate. It can be proven [45] that the same result is obtained if expanding the backward operator. In the case of the centred operator (4.6), one obtains:

$$\delta_t.q(t) = \dot{q}(t) + \mathcal{O}(k^2) \quad (4.9)$$

which states that this operator is more precise than the other two, being second order accurate. Finally, the same procedure can be used to find out the accuracy of the approximation of the second derivative (4.7), obtaining:

$$\delta_{tt} = \sum_{n=1}^{\infty} \frac{2k^{2(n-1)}}{(2n)!} \frac{d^{2n}}{dt^{2n}} = \frac{d^2}{dt^2} + \mathcal{O}(k^2) \quad (4.10)$$

which means that this operator is second order accurate too.

## 4.2 Simple Harmonic Oscillator

In order to obtain a discrete model for (3.37), it is possible to start by considering the lossless, unforced case: the simple harmonic oscillator (SHO).

$$\ddot{q}(t) = -\omega_0^2 q(t) \quad (4.11)$$

where  $\omega_0$  is the frequency of oscillation. A finite difference scheme for equation (4.11) can be obtained by using the operator (4.7) applied to the discrete series  $q^n$ :

$$\delta_{tt} q^n = -\omega_0^2 q^n \quad (4.12)$$

and expanding the operator yields

$$\frac{q^{n+1} - 2q^n + q^{n-1}}{k^2} = -\omega_0^2 q^n \quad (4.13)$$

Rearranging, one obtains the explicit recursion relation:

$$q^{n+1} = (2 - \omega_0^2 k^2) q^n - q^{n-1} \quad (4.14)$$

which is equal to that of a two-pole IIR digital filter. In fact, the corresponding frequency response consists of a single peak, centred around  $\omega_0$ .

In [45], Bilbao provides a thorough discussion on the discrete SHO and, by performing a frequency domain Von Neumann analysis he gets to the stability condition for the scheme (4.14)

$$k < (2/\omega_0) \quad f_s > \pi f_0 \quad (4.15)$$

In addition, Bilbao proves that, in the discretisation process, numerical approximations introduce an error in the oscillating frequency, which results being:

$$\omega = \frac{\cos^{-1}(1 - k^2 \omega_0^2 / 2)}{k} \quad (4.16)$$

Which is higher than the real frequency  $\omega_0$

### 4.2.1 Accuracy of the SHO

As before, Taylor expansions can be used to calculate the accuracy of the scheme (4.14). First, it is necessary to apply the discrete operators to a continuous function of time  $q(t)$ :

$$\delta_{tt}q(t) + \omega_0q(t) = 0 \quad (4.17)$$

Applying the formula for the accuracy of the second order operator in equation (4.10) to the equation above yields:

$$\frac{d^2}{dt^2}q(t) + \omega_0q(t) + \mathcal{O}(k^2) = 0 \quad (4.18)$$

Since the continuous SHO equation is of the form (4.11), it is clearly visible here the presence of an additional residual error, which is of order  $k^2$ . Thus, it is possible to say that scheme (4.14) is second order accurate.

### 4.2.2 Exact Scheme for the SHO

Once considerations over oscillating frequency and accuracy of the discrete scheme (4.14) have been investigated, it is possible to introduce a numerical integrator which exactly solves (4.11). This is, again, provided by Bilbao [45] and takes the form:

$$\left[ \delta_{tt} + \frac{2(1 - \cos(\omega_0k))}{k^2} \right] x^n = 0 \quad (4.19)$$

By expanding the operators, it is possible to obtain the recursion relation:

$$q^{n+1} = 2 \cos(\omega_0k)q^n - q^{n-1} \quad (4.20)$$

The precision of the actual oscillating frequency can be obtained by taking the  $z$  transform of (4.20):

$$z - 2 \cos(\omega_0k) + z^{-1} = 0 \quad (4.21)$$

The solutions of the equation above are:

$$z = e^{\pm i\omega_0k} \quad (4.22)$$

Therefore, the oscillating frequency is exactly  $\omega_0$ .

In order to calculate the accuracy, it is again possible to employ the Taylor expansion of the finite difference operator (4.7) applied to a continuous function of time  $q(t)$ . Expanding the operator inside square brackets in equation (4.19) and using (4.10) together with the cosine Taylor expansion yields:

$$\begin{aligned} & \sum_{n=1}^{\infty} \frac{2k^{2(n-1)}}{(2n)!} \frac{d^{2n}}{dt^{2n}} + (-1)^{n-1} \frac{2\omega_0^{2n}k^{2(n-1)}}{(2n)!} = \\ & = \sum_{n=1}^{\infty} \frac{2k^{2(n-1)}}{(2n)!} \left( \frac{d^{2n}}{dt^{2n}} + (-1)^{n-1} \omega_0^{2n} \right) \end{aligned} \quad (4.23)$$

Bringing out from the sum the common term

$$\frac{d^2}{dt^2} + \omega_0^2 \quad (4.24)$$

equation (4.19) can be rewritten in terms of big O notation:

$$(1 + \mathcal{O}(k^2)) \left( \frac{d^2}{dt^2} + \omega_0^2 \right) q(t) = 0 \quad (4.25)$$

The residual can be simplified out and, consequently, the relation above proves that scheme (4.19) solves the SHO exactly.

### 4.3 Lossy Oscillator

In order to simulate the modes of vibration, it is necessary to insert loss to the SHO equation. This can be achieved by adding a term dependent on the first time derivative, thus obtaining:

$$\ddot{q}(t) + \omega_0^2 q(t) + 2\sigma_0 \dot{q}(t) = 0 \quad (4.26)$$

which has the same form of equation (3.37), with no forcing. As mentioned in the previous chapter,  $\sigma_0 > 0$  is the damping parameter, which sets the decay rate for the system.

A finite difference scheme for equation (4.26) can be obtained in a similar way as for the SHO, by applying the difference operators (4.7), for the second order derivative and (4.6), for the first order derivative, to a discrete series  $q^n$ :

$$\delta_{tt}q^n = -\omega_0^2 q^n - 2\sigma_0 \delta t \cdot q^n \quad (4.27)$$

The expansion of the discrete operators yields the recursion relation for the lossy oscillator:

$$q^{n+1} = \frac{2 - \omega_0^2 k^2}{1 - \sigma_0 k} q^n - \frac{1 + \sigma_0 k}{1 + \sigma_0 k} q^{n-1} \quad (4.28)$$

With frequency domain Neumann analysis it is possible to obtain the stability condition for the scheme (4.28) [45]:

$$k < 2/\omega_0 \quad (4.29)$$

It is important to notice that this condition also provides a limit for  $\omega_0$  in relation to  $k$ . Therefore, when simulating the plate, the above relation also imposes a restriction over the maximum number of modes and, as a consequence, the values  $M_1$  and  $M_2$ , seen in equation (3.41). In particular, for a sampling frequency of  $f_s = 44100$  Hz, the highest possible mode results being  $f_{max} = 14037$  Hz.

### 4.3.1 Exact Scheme for the Lossy Oscillator

Previous paragraphs allowed to obtain a set of discrete rules which can be used to obtain a simulation of the plate modal equations (3.41) and (3.37), together with discrete values which allow to select a finite number of modes. Indeed, this approach is exactly the one employed by Ducceschi and Webb [32] for their EMT 140 simulation. Nevertheless, in a previous section it was seen that discretising the SHO by directly substituting the difference operators yields slightly inaccurate results, and that an exact integrator exists for the harmonic oscillator. As a matter of fact, an exact solution can be obtained also for the lossy oscillator, as it will be illustrated in this paragraph.

In order to obtain the exact integrator, one can start by considering the lossy equation (4.26) and then apply the variable transformation:

$$X(t) = e^{\sigma_0 t} q(t) \quad \rightarrow \quad q(t) = X(t) e^{-\sigma_0 t} \quad (4.30)$$

The chain rule for derivatives yields:

$$\frac{d}{dt} X e^{-\sigma_0 t} = \dot{X} e^{-\sigma_0 t} - X \sigma_0 e^{-\sigma_0 t} \quad (4.31)$$

and

$$\frac{d^2}{dt^2} X e^{-\sigma_0 t} = \ddot{X} e^{-\sigma_0 t} - \dot{X} \sigma_0 e^{-\sigma_0 t} - (\dot{X} \sigma_0 e^{-\sigma_0 t} - X \sigma_0^2 e^{-\sigma_0 t}) \quad (4.32)$$

By substituting into (4.26) and rearranging one obtains:

$$\ddot{X} + \tilde{\omega}_0^2 X = 0 \quad (4.33)$$

with

$$\tilde{\omega}_0 = \sqrt{\omega_0^2 - \sigma_0^2} \quad (4.34)$$

It appears clear that equation (4.33) has the form of a SHO, therefore, an exact scheme exists and is again given by (4.19), which, in the new variable  $X$ , takes the form:

$$X(t+k) + X(t-k) - 2X(t) \cos(\tilde{\omega}_0 k) = 0 \quad (4.35)$$

Substituting back for  $q(t)$  yields:

$$q(t+k) = 2e^{-\sigma_0 k} \cos(\tilde{\omega}_0 k) q(t) - e^{-2\sigma_0 k} q(t-k) \quad (4.36)$$

If a discrete series  $q^n$  is used instead of a continuous function, one obtains the recursion relation which exactly solves the lossy oscillator

$$q^{n+1} = 2e^{-\sigma_0 k} \cos(\tilde{\omega}_0 k) q^n - e^{-2\sigma_0 k} q^{n-1} \quad (4.37)$$

Finally, the scheme above takes a operator form:

$$\left( \delta_{tt} + \frac{2e^{-\sigma_0 k}}{k^2} (e^{\sigma_0 k} - \cos(\tilde{\omega}_0 k)) + \frac{e_{t-}}{k^2} (e^{-2\sigma_0 k} - 1) \right) q^n = 0 \quad (4.38)$$

Through Taylor expansion, it is possible to prove that the integrator above provides an exact solution to the oscillator (4.26).

Before being ready to introduce an input signal, it is necessary to make some considerations on the stability condition for the exact scheme (4.38). This can be achieved by employing a frequency domain Von Neumann analysis. Considering the recursion (4.37), the first thing to do is to insert a test solution  $q^n = z^n$ , with  $z = e^{sk}$  and  $s$  being a complex frequency. By doing this, one obtains the characteristic equation:

$$z - 2e^{-\sigma_0 k} \cos(\tilde{\omega}_0 k) + e^{-2\sigma_0 k} z^{-1} = 0 \quad (4.39)$$

Rearranging, the relation above takes the form of the quadratic equation

$$z^2 - 2e^{-\sigma_0 k} \cos(\tilde{\omega}_0 k) z + e^{-2\sigma_0 k} = 0 \quad (4.40)$$

Following Bilbao [45], stability is ensured if the roots of the characteristic equation are bounded by unity and, since the one above is a quadratic equation this is true if:

$$| -2e^{-\sigma_0 k} \cos(\tilde{\omega}_0 k) | - 1 \leq e^{-2\sigma_0 k} \leq 1 \quad (4.41)$$

Which is true for any  $k$ .

Therefore, the use of the exact scheme allows not to impose any limit on the maximum number of modes, contrary to what happened with the non-exact scheme, where the maximum frequency of vibration was given by (4.29). This allows to keep each normal mode up to the limit of the audio band (it is not necessary to go further, as it would be a waste of computational power).

### 4.3.2 Forcing

Everything said until now is valid in the case of unforced oscillators, nevertheless, in order to obtain an outgoing sound it is necessary to provide an excitation for the scheme. The forced oscillator takes the form:

$$\ddot{q}(t) + \omega_0^2 q(t) + 2\sigma_0 \dot{q}(t) = p(t) \quad (4.42)$$

Where the time function  $p(t)$  represents an input signal. For equation (4.42) an exact integrator does not exist, however, it is possible to expand equation (4.38) in Taylor series and add a number of terms to the external forcing, in order to obtain a correction up to a desired order. Doing this yields:

$$G(k) \left( \frac{d^2}{dt^2} + 2\sigma_0 \frac{d}{dt} + \omega_0^2 \right) q^n = 0 \quad (4.43)$$

where

$$G(k) = 1 - \sigma_0 k + \frac{k^2}{12} \left( \frac{d^2}{dt^2} + 2\sigma_0 \frac{d}{dt} + 8\sigma_0^2 - \omega_0^2 \right) + \mathcal{O}(k^3) \quad (4.44)$$

By substituting the derivatives with discrete operators, it is possible to obtain a correction to the input signal in the form

$$p(t) \rightarrow \left( 1 - \sigma_0 k + \frac{k^2}{12} (\delta_{tt} + 2\sigma_0 \delta_t + 8\sigma_0^2 - \omega_0^2) \right) p^n \quad (4.45)$$

#### 4.4 An Update Equation for the Modes

The last paragraphs allowed to derive all the tools for writing an (almost) exact numerical integrator for calculating a single mode on MATLAB, as it will be shown later on. It is important to notice that, if expanding the operators in (4.45), a future point  $p^{n+1}$  is needed, which, of course, is not known. However, it is simply possible to shift the whole series one sample back without affecting the outgoing sound, indeed, doing this simply introduces a one-sample delay in the output, which is not perceived by the ear. The recursion relation for a single mode  $q_{m_1, m_2}$  takes the form:

$$\begin{aligned} q_{m_1, m_2}^{n+1} = & 2e^{-\sigma_0 k} \cos(\tilde{\omega}_0 k) q_{m_1, m_2}^n - e^{-2\sigma_0 k} q_{m_1, m_2}^{n-1} + \frac{1 - \sigma_0 k}{12} p_{m_1, m_2}^n + \\ & + \left( \frac{5}{6} - \sigma_0 k + \frac{2}{3} - \sigma_0^2 k^2 - \frac{\omega_0^2 k^2}{12} \right) p_{m_1, m_2}^{n-1} + \frac{1 - \sigma_0 k}{12} p_{m_1, m_2}^{n-2} \end{aligned} \quad (4.46)$$

Where the exciter  $p_{m_1, m_2}^n$  consists of:

$$p_{m_1, m_2}^n = \frac{\Phi_{m_1, m_2}(x_p, y_p)}{\rho H} P^n \quad (4.47)$$

and  $P^n$  is a sampled version of the input signal. In order to retrieve the output signal, a number of these update equations equal to the maximum number of modes need to be calculated in parallel. Then, the displacement at the output point can be obtained through the use of equation (3.41).

## Chapter 5

# Optimisation

In the previous chapters, a complete computational model for the EMT 140 plate has been presented, which includes a physical model for damping and employs a modal decomposition, then simulated by using an exact numerical integrator. With the configuration previously detailed, the resulting number of modes is above 20000 and, unfortunately, calculating such a high number of oscillators in parallel in real time is beyond the capabilities of most modern devices. In [32], Ducceschi and Webb proposed a method for discarding less perceptually relevant modes which is based on psychoacoustic considerations, later employed also by Willemssen et al. [33]. This technique finds itself on the logarithmic nature of human hearing: since the modes of vibration are approximately evenly spaced along the frequency axis, this means that in a higher octave band more modes will be present. Thus, it is possible to discard higher modes without too much effect on the output quality.

In this work, it was decided to employ a different method, based on least squares optimisation, which is in part similar to the one proposed by Maestre et al. [56]. The idea behind this solution is to calculate the analytic impulse response of the plate, starting from the modal decomposition, select the most relevant peaks from the magnitude spectrum and perform least squares approximation to find the new modal weights, in fact, as it will be shown later, the input and output modes can be considered as a single one. In this chapter, this process will be detailed: first, some considerations on least squares approximation will be made, then it will be explained how this method was used in the context of this work.

### 5.1 Least Squares Regression

Least Squares (LS) is a form of linear optimisation. Considering a set of measurements  $y_n$ , taken for different known parameter values  $x_n$  (explanatory variables), least squares starts from the assumption that these can be linked by a linear rela-

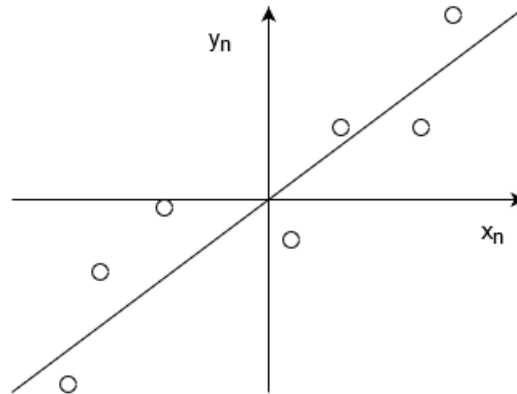


**Figure 5.1:** Graphical visualisation of the least squares data model.

tion, however, the  $y_n$  are affected by some measurement noise  $\epsilon_n$ . Therefore, it is possible to write:

$$y_n = px_n + \epsilon_n \quad (5.1)$$

Where  $p$  is a scalar weight (or slope). LS regression aims to find the  $p$  which minimises the sum of squared errors:

$$\eta(p) = \frac{1}{2} \sum_{n=1}^N (y_n - px_n)^2 \quad (5.2)$$

Essentially, what LS looks for is the best slope which fits the measurements, as shown in Figure 5.1. Equation (5.2) can be written in vector form as.

$$\eta(p) = \frac{1}{2} \|\mathbf{y} - p\mathbf{x}\|^2 \quad (5.3)$$

Considering the norm as the Euclidean one, and writing it as an inner product:

$$\eta(p) = \frac{1}{2} (\mathbf{y} - p\mathbf{x})^T (\mathbf{y} - p\mathbf{x}) \quad (5.4)$$

In order to find the proper weights, it is possible to derive the expression above, set it equal to zero and solve for  $p$ . The fact that the error is a quadratic function of  $p$ , and that what multiplies  $p^2$  must be positive ensures that the found value will be a minimum. Taking into account the linearity of the transposition operator one then obtains:

$$p_{opt} = \frac{\mathbf{y}^T \mathbf{x}}{\mathbf{x}^T \mathbf{x}} \quad (5.5)$$

Which is a solution to the LS problem.

### 5.1.1 Multiple Explanatory Variables

A more complex case is encountered when the measurements depend on more than one explanatory variable, and, as a consequence, multiple weights need to be found. This situation takes the math form

$$y_n = \sum_m p_m (x_n)_m + \epsilon_n \quad (5.6)$$

In this case, the error function to minimise becomes:

$$\eta(\mathbf{p}) = \frac{1}{2} \|\mathbf{y} - \sum_m p_m \mathbf{x}_m\|^2 \quad (5.7)$$

It is now possible to define the matrix  $X$ , whose columns are made of the explanatory vectors, meaning that to each column will correspond one  $p_m$ . Thus, the error function can be written:

$$\eta(\mathbf{p}) = \frac{1}{2} \|\mathbf{y} - X\mathbf{p}\|^2 \quad (5.8)$$

Which, again, can be written in an inner product form

$$\eta(\mathbf{p}) = \frac{1}{2} (\mathbf{y} - X\mathbf{p})^T (\mathbf{y} - X\mathbf{p}) \quad (5.9)$$

Even though matrices are now considered, it is still possible to use calculus to find the analytic solution to the LS problem. Deriving the error function with respect to  $\mathbf{p}$ , imposing it equal to zero and solving yields a solution similar to (5.5):

$$\mathbf{p}_{opt} = (X^T X)^{-1} X^T \mathbf{y} \quad (5.10)$$

### 5.1.2 Complex Variables

As it will be illustrated in the next paragraph, it is of interest the case where the data vector  $y$  and the explanatory variables  $X$  are complex, while the weights  $\mathbf{p}$  are real. In this case, considering the complex norm, the error function becomes:

$$\eta(\mathbf{p}) = \frac{1}{2} \|\Re(\mathbf{y}) - \Re(X\mathbf{p})\|^2 + \frac{1}{2} \|\Im(\mathbf{y}) - \Im(X\mathbf{p})\|^2 \quad (5.11)$$

Again, by expanding the norms, deriving with respect to  $p$  and imposing everything equal to zero one obtains:

$$\mathbf{p}_{opt} = (\Re(X^T)\Re(X) + \Im(X^T)\Im(X))^{-1} (\Re(X^T)\Re(\mathbf{y}) + \Im(X^T)\Im(\mathbf{y})) \quad (5.12)$$

## 5.2 Modes Optimisation

Following the approach proposed by Maestre et al. [56], it was chosen to perform an optimisation over the frequency domain. The basic idea is to calculate the analytic frequency response of the plate, in order to obtain a representation in the frequency domain, find the most prominent peaks, their bandwidth and their frequency location and, finally, build another frequency response using only those peaks. As it will be illustrated, the peaks heights are given by the modal weights, which are relative to each eigenfrequency. With this method, single eigenfrequencies are "lost", meaning that the new peaks will not necessarily correspond to the analytic modes. For this reason, new modal weights need to be found: the least squares technique will be used for this purpose.

### 5.2.1 Frequency Response

The first step for the optimisation is to calculate the frequency response of the plate in the continuous domain. To do this, the Fourier transform of the modal equations obtained in chapter 3 will be calculated.

In order to obtain the frequency response it is possible to start considering the single mode  $(m_1, m_2)$  equation (3.37) previously obtained, when the input has the impulsive form

$$P(t) = \delta(t - t_0) \quad (5.13)$$

Under this condition, taking the Fourier transform yields:

$$-\omega^2 Q_{m_1, m_2}(\omega) + \omega_{m_1, m_2}^2 Q_{m_1, m_2}(\omega) + 2i\omega\sigma_{m_1, m_2} Q_{m_1, m_2}(\omega) = \frac{\Phi_{m_1, m_2}(x_p, y_p)}{\rho H} \quad (5.14)$$

Solving for  $Q(\omega)$  one obtains the frequency response of a single mode

$$Q_{m_1, m_2}(\omega) = \frac{1}{\rho H} \frac{\Phi_{m_1, m_2}(x_p, y_p)}{(\omega_{m_1, m_2}^2 - \omega^2 + 2i\omega\sigma_{m_1, m_2})} \quad (5.15)$$

In order to calculate the output of the whole system in the frequency domain, it is useful to consider the case where the equation consists of a single mode, in which case the equation (3.41) becomes:

$$u(x_o, y_o, t) = q(t)\Phi(x_o, y_o) \quad (5.16)$$

Since the modes do not depend on time they are not affected by the transformation, therefore taking the Fourier transform becomes:

$$U(x_o, y_o, \omega) = Q(\omega)\Phi(x_o, y_o) \quad (5.17)$$

where  $Q(\omega)$  is given by (5.15). With the help of the linearity property of the Fourier transform it is possible to extend the equation above to the full case, thus obtaining the complete frequency response of the plate in the continuous domain.

$$U(x_o, y_o, \omega) = \sum_{m_1=1}^{M_1} \sum_{m_2=1}^{M_2} \frac{1}{\rho H} \frac{\Phi_{m_1, m_2}(x_p, y_p) \Phi_{m_1, m_2}(x_o, y_o)}{(\omega_{m_1, m_2}^2 - \omega^2 + 2i\omega\sigma_{m_1, m_2})} \quad (5.18)$$

Looking at the equation above, it is important to notice that the input-output modes are now combined into a single coefficient, which can be defined as

$$\Phi_{m_1, m_2}^{TOT} := \frac{\Phi_{m_1, m_2}(x_p, y_p) \Phi_{m_1, m_2}(x_o, y_o)}{\rho H} \quad (5.19)$$

This coefficient is the one that sets the modes height. Finally, equation (5.18) can be rearranged:

$$U(x_o, y_o, \omega) = \sum_{m_1=1}^{M_1} \sum_{m_2=1}^{M_2} X_{m_1, m_2}(\omega) \Phi_{m_1, m_2}^{TOT} \quad (5.20)$$

where

$$X_{m_1, m_2}(\omega) := \frac{1}{\omega_{m_1, m_2}^2 - \omega^2 + 2i\omega\sigma_{m_1, m_2}} \quad (5.21)$$

### 5.2.2 Least Squares

In order to perform least squares it is first necessary to discretise the frequency axis, obtaining a vector  $\omega_i$  with  $i = 1, 2, 3, \dots, N$  and  $\omega_N / (2\pi) = 20$  kHz. This way, one gets a number of observations from the actual impulse response (5.20):

$$U[\omega_i] = \sum_{m_1=1}^{M_1} \sum_{m_2=1}^{M_2} X_{m_1, m_2}[\omega_i] \Phi_{m_1, m_2}^{TOT} \quad (5.22)$$

In vector form, the equation above becomes:

$$\mathbf{y} = X\Phi^{TOT} \quad (5.23)$$

where  $X$  is a matrix whose columns contain the frequency observations for each mode, and  $\Phi^{TOT}$  is a column vector containing the total modal weights correspondent to each mode. Following the least squares formulation (5.6), it is possible to consider  $\mathbf{y}$  as the measurements vector, which in this case contains the target.

### Finding Modal Peaks

At this point, it is necessary to examine  $\mathbf{y}$  for finding the most prominent peaks. In the algorithm, this is achieved by using the MATLAB function `findpeaks`, which

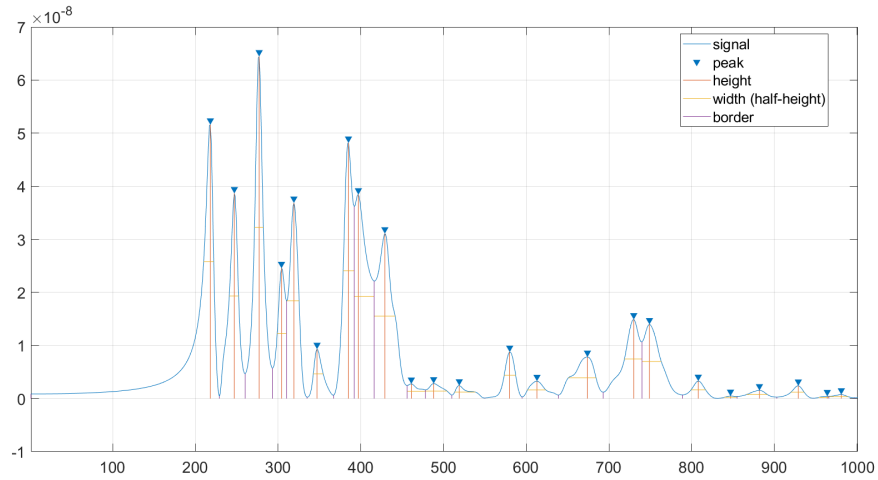


**Figure 5.2:** Results provided by the `findpeaks` function applied to a section of the target frequency spectrum.

returns the local maxima of a vector and their bandwidth. The function is run over the magnitude spectrum, the absolute value of  $\mathbf{y}$

The function is set to measure the peaks widths at half height, in fact, this quantity is linked to the damping factor. Given a peak bandwidth  $w$  and center frequency  $\omega_0$ , it is possible to define the Q-factor as:

$$Q = \frac{\omega_0}{w} \quad (5.24)$$

The damping coefficient is then calculated using

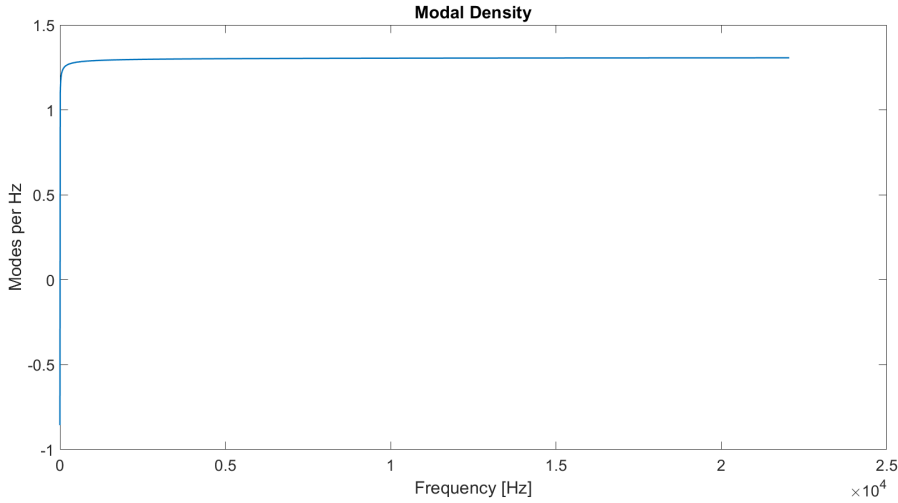
$$\sigma_0 = \frac{1}{4Q} \quad (5.25)$$

Figure 5.2 shows the results of the `findpeaks` function applied to a section of the target frequency spectrum.

### Modes Rejection

Once the frequency peaks and their bandwidth have been obtained, it is possible to reject some of them, in particular the least prominent, for further optimisation. In order to do this, the target frequency response is divided into frequency bands, and each band is singularly analysed with `findpeaks`.

There are different ways to split the frequency axis. One, employed by Maestre [56], is to exploit the logarithmic nature of human hearing and subdivide the frequencies in a log scale. In particular, Maestre makes use of the *Bark scale*, which



**Figure 5.3:** Modal density of the EMT 140 in modes per Hertz, calculated with the relation provided by Arcas [31].

consists of 24 frequency bands, called *critical bands*, based on psychoacoustic principles. The Bark scale is linear below 500 Hz and approximately logarithmic above. Because of this structure, the width of higher bands is greater in terms of Hertz, this results in cutting more frequencies in the higher parts of the spectrum. The bark scale approach is based on the idea that, since human hearing is logarithmic, higher octaves contain more modes, thus, cutting more high frequencies will not impact the quality of the output .

Another possible method is to split the frequency axis in linear bands, and cut an equal number of modes from each. This approach founds itself on the fact that the EMT 140 possesses an approximately constant modes density [31], as it is possible to see in Figure 5.3. Thus, rejecting the same number of frequencies from evenly subdivide bands will not affect this property. In this work, both methods were implemented and results obtained with the two approaches will be provided in chapter 6.

### Optimised Impulse Response

With the selected peaks it is possible to calculate the new optimised impulse response. If the optimal modes are called  $\omega_k$ , with  $k = 1, 2, \dots, M_o$ ;  $M_o$  being the total number of optimal modes, it is possible to write:

$$X_k[\omega_i] := \frac{1}{\omega_k^2 - \omega_i^2 + 2i\omega_i\sigma_k} \quad (5.26)$$

Hence, the optimised impulse response, written in vector form becomes:

$$U^{opt} = X_k \Phi_k^{opt} \quad (5.27)$$

However, it is now clear that the optimal modal weights  $\Phi_k^{opt}$  are still missing. Nevertheless, the least squares problem to be solved is shaping up: the matrix  $X$  can be considered as the explanatory variable which, when multiplied by a scalar weight  $\Phi^{opt}$  needs to get close to the observation  $y$ . Hence, the LS error function to be minimised becomes:

$$\eta(\Phi^{opt}) = \frac{1}{2} \|y - X\Phi^{opt}\|^2 \quad (5.28)$$

Both  $y$  and  $X$ , being frequency responses, are complex, however, the modal weights need to be real by definition. Thus, the problem is solved by using equation (5.12) obtained in the previous section.

## Chapter 6

# Results & Evaluation

This chapter will illustrate two different methods that were used to evaluate the algorithm. One, the technical evaluation, is based on analysis of measurements and the other, the perceptual test, is based on a questionnaire. Unfortunately, during the course of the project, there was no access to an actual EMT 140 plate reverb unit; therefore, it was impossible to make a thorough comparison between the model and the device. In particular, extensive measures on the quality of the damping model implemented could not be carried out, as no reference sound was available. One way to test the sound quality of the algorithm could have been to compare it with other commercial plugins based on physical models, such as the Physical Audio PA1, or the UVI Plate; in particular, the latter features a physical model of damping as well. Nevertheless, since the plugins are not open-source, it would have been complicated to understand the reasons for any discrepancies in terms of sound quality; moreover, making a comparison with other simulations would not have provided much useful information. Consequently, extensive tests on the algorithm sound quality and the performances of the damping model are left for future work, and the testing focused on the the optimisation. In particular, the technical evaluation consisted in measuring the differences between the frequency responses of the plate with all the modes, and the optimised versions of it. In the perceptual test, subjects were asked to listen to different audio files to which the reverb was applied, in different optimisation versions. Then, they had to rate how much difference they perceived with a reference audio, made with the full plate. While processing the audio files, the running times were also measured, in order to understand if the plate could be operated in real-time.

### 6.1 Measurements Setup

In order to test the optimisation performances, the plate parameters were set to be always the same, this way no bias was introduced. The algorithm allows to choose

whether to output a mono or a stereo signal, the latter is obtained by simply enabling another virtual accelerometer placed at a different position on the plate, as it happens on the real EMT 140. This allows to produce interesting sounds, perceptually speaking; nevertheless, each accelerometer has its own frequency response, therefore, it would have been necessary to analyse each one of them separately, something which would not have added meaningful information to the tests. For this reason, all the testing were conducted by enabling only one accelerometer. Below are listed all the physical parameters used for the tests.

- Horizontal Length:  $L_x = 2$  m.
- Vertical Length:  $L_y = 1$  m.
- Thickness:  $H = 0.5$  mm.
- Input Position:  $(0.52L_x, 0.53L_y)$ , chosen following Ducceschi and Webb [32].
- Output Position:  $(0.47L_x, 0.62L_y)$ , again following Ducceschi and Webb.
- Material: Carbon Steel SAE 1010. For which:  $E = 2 \times 10^{11}$  Pa,  $\nu = 0.3$ ,  $\rho = 7.872 \times 10^3$  kg/m<sup>3</sup>.
- Distance of the porous panel: 0.03 m. Chosen to be half-way between the possible extremes positions in the real device.

As seen in chapter 3, the damper model by Cummings showed trends more similar to the one reported by Arcas. Nevertheless, it also presented some troubles in calculating the damping coefficients in the lower frequencies. For this reason, the damper model by Craik was used during the testing.

## 6.2 Frequency Bands & Modes Rejection

Modes rejection in this algorithm works this way: the computed, full (containing all the modes) frequency response is divided into frequency bands as explained in chapter 5; then, for each band, the `findpeaks` function is run, which outputs all the found peaks, their location and their width. Once all this data is obtained, it is possible to reject some of the peaks found, in particular the least prominent ones. This is done based on a variable that sets the maximum number of peaks per frequency band, and needs to be set by the user, depending on the desired grade of optimisation. In the testing, this parameter was chosen empirically: first, it was checked the number of modes per band found by `findpeaks`, then the peaks limit was reduced until the algorithm could run in real-time.

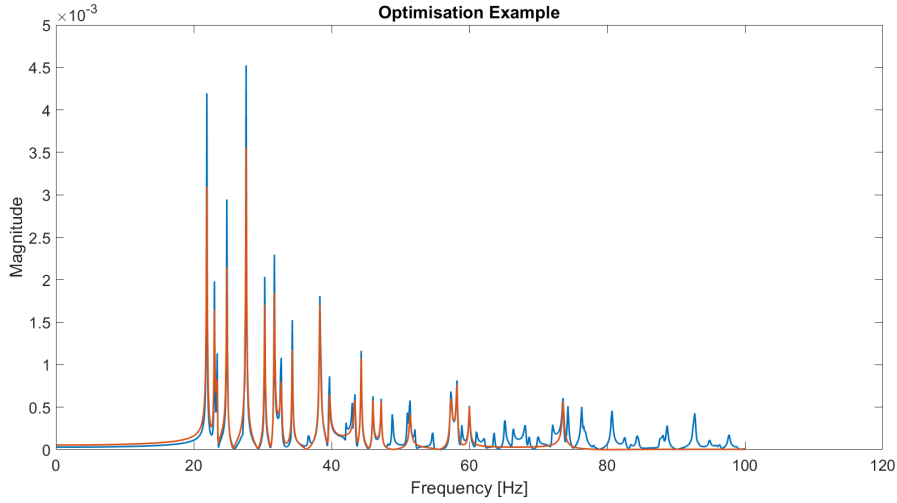


**Figure 6.1:** Example of the optimisation run on the first linear band, with the maximum modes number per band set to 20. The blue line indicates the full plate frequency spectrum, the orange line is the optimised one.

As previously said, two different ways of splitting the frequency axis were employed, one logarithmic-based and one linear-based. The first follows the Bark scale, which consists of 24 critical bands, whose limits are:

$$[20, 100, 200, 300, 400, 510, 630, 770, 920, 1080, 1270, 1480, 1720, 2000, 2320, 2700, 3150, 3700, 4400, 5300, 6400, 7700, 9500, 12000, 20000] \quad (6.1)$$

The lowest and highest values were set to be limits of the audio band. As it was mentioned above, this scale is based on the logarithmic nature of the human hearing; therefore, higher octaves contain more frequencies and, in this case, modes. For this reason, by using the Bark scale, the rejected modes will be mostly in the higher part of the spectrum. The maximum numbers of peaks chosen for the experiments with the Bark scale were 600 and 300. The first one was selected because it allowed to run the algorithm in real-time, while still maintaining a high sound quality, the latter was chosen to observe how much quality was lost by rejecting a high number of modes.

The other frequency splitting method employed was linear. As before mentioned, this scale was chosen in order to preserve the constant modes density, which is a characteristic of the EMT 140. In this case, the frequency axis was split linearly in bands large 100 Hz. As expected, since the bands are thinner than in the Bark scale, the modes numbers were much lower than in the other case. Therefore, the maximum number of peaks selected in this case were 20 and 10, chosen with the same criteria explained above. Figure 6.1 illustrates an example of the optimised frequency response; here a linear splitting was performed and a maximum

number of 20 peaks per band was set. It is possible to see how the less prominent peaks are being ignored.

### 6.2.1 Running Times

Before moving to the measurements results, it is necessary to make some considerations over the running speed of the algorithm. In order to calculate it, it was measured the time taken by the audio loop for processing a 5-seconds impulse with the MATLAB `tic toc` function. It should also be pointed out that these measurements were obtained with the mono version of the algorithm, and that a stereo sound requests more time to run. Nevertheless, in order to obtain a proper real-time version of this model, it would be necessary to make a porting to C++, and the use of this language would allow to perform many more low-level optimisations to speed up the code, with respect to MATLAB.

Full	No Cut	Bark 600	Bark 300	Linear 20	Linear 10
20.433976 s	8.628766 s	3.906116 s	2.577829 s	4.132802 s	2.017438 s

**Table 6.1:** Times in seconds to process a 5-seconds impulse by various versions of the algorithm

Table 6.1 shows the measured times taken by the audio loops for processing a 5-seconds impulse. In particular, "Full" refers to the plate with all the modes, "No Cut" indicates an optimised version of the plate with no peaks rejected, obtained with linear splitting, meaning that all the peaks found by `findpeaks` were kept. "Bark 600" and "Bark 300" refer to the optimisation obtained by dividing the frequency axis with the Bark scale, and setting the maximum peaks number to 600 and 300 respectively. Similarly, "Linear 20" and "Linear 10" refer to the linear splitting of the frequency axis, and the numbers indicate the maximum modes per band that were set. It can be noticed how all the performed optimisations allowed to run the model in real-time: in fact, the processing time is lower than the 5 seconds of the requested signal. On the contrary, both the full plate and the "No Cut" versions would not allow to perform real-time computation. In particular, the time requested to compute the full plate output is more than four times higher than the length of the requested signal.

## 6.3 Technical Evaluation

In order to perform a technical evaluation, it was decided to compare the frequency responses of the full plate and the optimised versions, which are both computed during the optimisation process. The comparison was performed following a paper by Ryder [57], in which the correlation coefficient is used for frequency response

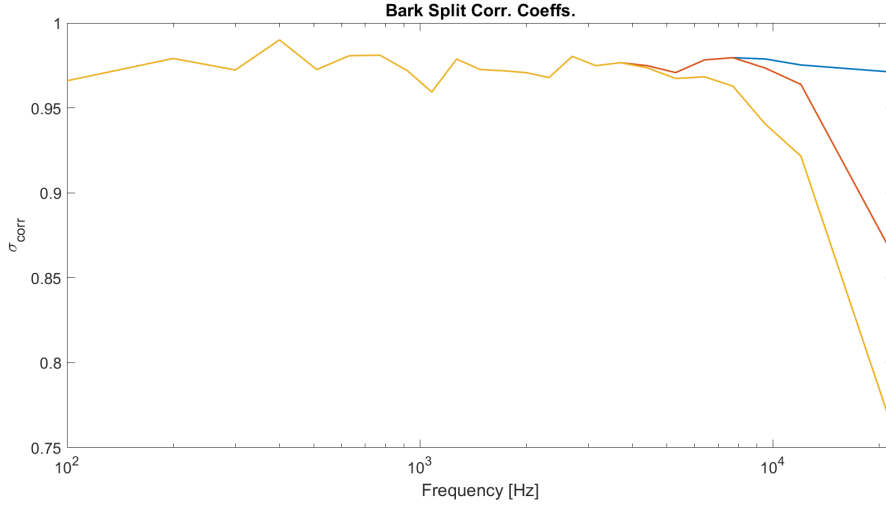


**Figure 6.2:** Correlation coefficients for each Bark band. The blue line is relative to the "No Cut" version, the orange line to the "600" version and the yellow one to the "300" version.

analysis. Ryder defines the correlation coefficient as:

$$\sigma_{corr} = \frac{\sum_{x=1}^N x_i y_i}{\sqrt{\sum_{x=1}^N x_i^2 \sum_{x=1}^N y_i^2}} \quad (6.2)$$

In this case,  $X = x_1, x_2, \dots, x_N$  and  $Y = y_1, y_2, \dots, y_N$  are the magnitudes of the frequency responses of the optimised and full plate respectively. The correlation coefficient has values between  $-1$  and  $1$ , where  $1$  indicates perfect correlation, namely  $X$  and  $Y$  are identical,  $0$  indicates absence of correlation and  $-1$  negative correlation. Therefore, the closer  $\sigma_{corr}$  is to  $1$  the better it is. For each optimised version, it was decided to compute the correlation coefficient for both the whole spectrum and for the single frequency bands, in order to check where the modes are cut the most. The next paragraphs will illustrate the results of the measurements performed. For both the Bark and the linear splitting will be reported: the correlation coefficient of the "No Cut" version, and the two optimised versions with the modes limited.

### 6.3.1 Bark Bands

Figure 6.2 shows the correlation coefficients of the Bark optimised plates, for each frequency band. For each line, the correlation is calculated with respect to the full plate frequency response, calculated with all the modes. It is clearly visible how, by employing this scale, modes are cut only in the highest part of the spectrum, in fact the correlation coefficients drop in the highest bands when a maximum number of

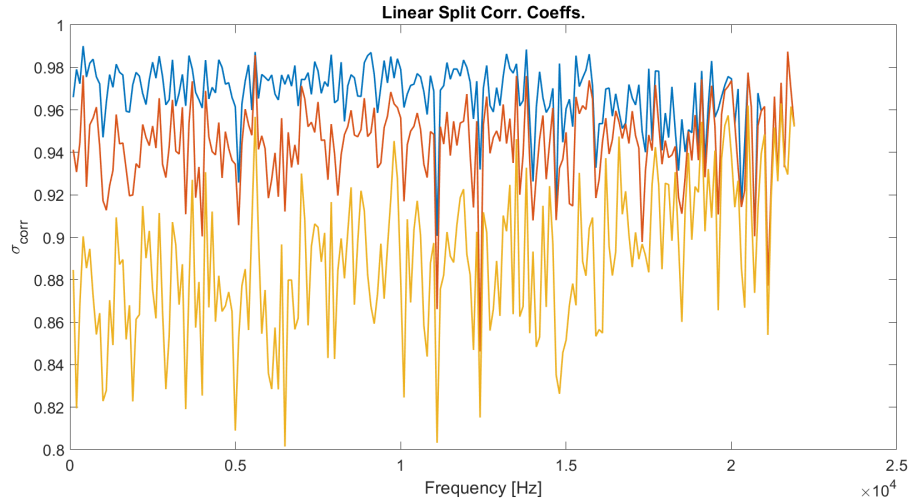


**Figure 6.3:** Correlation coefficients for each Linear band. The blue line is relative to the "No Cut" version, the orange line to the "20" version and the yellow one to the "10" version.

modes is set. Nevertheless, this method allows to maintain a high grade of fidelity until around 10 kHz, if at least 300 modes per band are kept. As a matter of fact,  $\sigma_{corr}$  remains above 0.95 under that frequency.

Besides the correlation per band, it was also calculated an overall correlation coefficient for each version by taking into account the whole spectrum; these are shown in Table 6.2. It can be seen how, by considering the full spectrum at once, the optimisation did not reflect much on the value of  $\sigma_{corr}$ . This means that, even when a high number of peaks is cut, such as in the "300" case, a overall high grade of fidelity is maintained.

No Cut	Bark 600	Bark 300
$\sigma_{corr} = 0.966459323$	$\sigma_{corr} = 0.966451306$	$\sigma_{corr} = 0.966438318$

**Table 6.2:** Correlation coefficients for the full frequency responses of the Bark optimised plates

### 6.3.2 Linear Bands

Figure 6.3 shows the correlation coefficients of the linear optimised plates. In this case the plot is more messy, as the number of bands is much higher. Nevertheless, it can be seen how the optimisation in this case lowers the correlation coefficient in the whole spectrum, in fact, peaks are not cut only in a specific area anymore. In the "10" case, the coefficient is even lower at lower frequencies, indicating that findpeaks found more peaks in that region, hence, more modes are rejected.

The overall correlation coefficients are reported in Table 6.3. Here, it is visible how the linear optimisation yields a lower overall  $\sigma_{corr}$ , in fact, the coefficients relative to the Bark optimised versions are higher than the ones obtained with the linear optimisation. Since, as seen in Table 6.1, the running times are similar for the two optimisation versions, the correlation results suggest that the Bark scale might be the best choice for optimising the plate. Nevertheless, this will need to be confirmed by the perceptual test, in fact, cutting more on the high frequencies might result in a non desirable timbre change.

No Cut	Linear 20	Linear 10
$\sigma_{corr} = 0.966460369$	$\sigma_{corr} = 0.940931853$	$\sigma_{corr} = 0.882173353$

**Table 6.3:** Correlation coefficients for the full frequency responses of the Linear optimised plates

## 6.4 Perceptual Test

Along with the technical evaluation, also a perceptual test was carried out, in order to observe the effects of the optimisation on the perceived sound, and if subjects could hear differences between the two kind of optimised plates. The test was structured with a MUSHRA method [58]; the name stands for Multiple Stimuli with Hidden Reference and Anchor, and it is an experiment methodology originally designed for testing audio compression. In this evaluation, subjects are provided a reference audio file, which is uncompressed and it is specified to be the reference. Then, testers need to rate several compressed versions of the first audio, without knowing the compression characteristics. Among the files to rate are included: a copy of the reference file and at least one anchor file, which is another copy of the first file, lowpassed at 3.5 kHz. It is specified that audio clips should not be longer than 20 seconds to avoid fatiguing of listeners and to reduce the total duration of the test.

In this test, three audio clips were used: a drum loop, an acoustic guitar riff and some vocals. The drums were recorded with the *Modo Drum* plugin,<sup>1</sup> by *IK Multimedia*, the guitar and vocals were downloaded from a sample library. Attention was payed to make sure that the audios were not already reverberated. The files lengths were, respectively: 12, 9 and 11 seconds. It was decided to select single instrument clips, in order for the subjects to have less instruments to focus on at the same time. Drums and vocals were selected as it was seen that online reviews of reverbs, in particular of plate reverb plugins, typically use these instruments sounds for testing; an acoustic guitar was chosen too because it has a very well known timbre. For each audio clip, eight files were presented to the testers.

<sup>1</sup>[www.ikmultimedia.com/products/mododrum](http://www.ikmultimedia.com/products/mododrum)

One was the reference file, placed first in the list, which consisted in the audio clip processed with the full plate. The latter seven were: an hidden reference file, the 300 and 600 Bark and the 20 and 10 linear optimised versions, the linear "No Cut" version (chosen because it has the highest correlation coefficient among the two No Cut versions) and the anchor, made by lowpassing the reference file at 3.5 kHz. The order of the files to rate was randomised, so for each clip the position of the various versions was not the same, this in order not to introduce any form of bias.

After collecting personal data, such as age, gender and education, users were asked to indicate their experience with music, in particular, if they played an instrument, how much music they listened to per day and if they had any experience in music recording or producing. After these questions, subjects were shown three screens, one for each instrument, where the eight clips were presented one below the other. Here, they were asked to rate the files from the second to the eighth compared to the first one, by using sliders in a range from 0 to 100, where 0 was said to mean "bad quality" and 100 "excellent quality". After the rating section, as a last question, testers were presented the dry (with no reverberation applied) drum loop and the fully wet (reverberated) version of it, made with the full plate. They were then asked to indicate their general opinion on the reverberation effect. This was done to collect some thoughts on the quality of the reverberation effect, even though, as previously said, more thorough testing on the reverb sound need to be performed. Since the survey had to be run from remote due to Covid-19 related restrictions, participants were asked wear headphones for the test, and to indicate the model. The questionnaire was implemented and run using PsyToolkit [59, 60], a free-to-use toolkit for programming and running surveys, chosen because it allows to easily upload media files. Unfortunately, the toolkit did not allow to personalise much the GUI, and all the files had to be presented together, included the reference. This fact introduced some confusion in some participants, in particular some of them reported that it had been difficult to identify the reference file. Moreover, since the test had to be conducted remotely, no clarification about this issue could be provided during the course of the test. Another problem arose in the displaying of the length of the audio clips, in particular, for some of them it was much longer than the real one, nevertheless, the files played normally. Information about this issue was provided before starting the test.

### 6.4.1 Survey Results

In total, twelve people participated to the test, they were between 23 and 47 years old, with a mean age of 29. All the participants except one had at least a Bachelor's Degree, some in engineering and others in arts. Among the participants, 10 either played an instrument for more than 4 years, or are used to listen to music for at least 2 – 3 hours a day. The instruments played by the subjects are of various kinds,

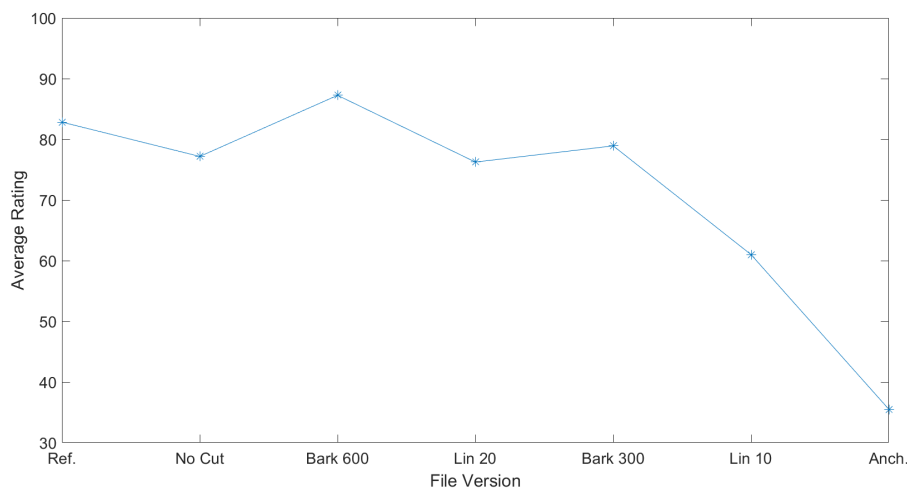


**Figure 6.4:** Average ratings for the drum samples. From left to right: Hidden Reference, No Cut, Bark 600, Linear 20, Bark 300, Linear 10, Anchor.

and included the test samples instruments: drums, guitars and vocals. Moreover, seven participants stated to have experience in music production and/or recording. Eleven subjects stated to have used over-ear headphones during the questionnaire, of various brands, whereas one used in-ear ones.

### Drum Samples

Figure 6.4 displays the average ratings for the drum samples. The graph provides many information: first of all, the anchor got an overall low rate. This is a good fact: this file was missing all the high frequencies, and this rating means that testers payed attention to these details. The second interesting detail which emerges from the picture is that the Bark 600 version got a rating which is higher than both the No Cut version and the hidden reference. Even though this result could be biased by many testing uncertainties, such as the different headphones used by the subjects, or the different environment in which they were, it indicates that the Bark optimisation yields surprisingly good results. This is confirmed by the fact that also the Bark 300 version got an higher rating with respect to both the linear versions, even though Bark 300 has a higher level of optimisation than the Linear 20, as it is reported in Table 6.1. These results act also as a confirm that the correlation studies yielded accurate results, in fact, the overall correlation coefficient of the Bark 300 optimised spectrum is higher than the one relative to the Linear 20 version, this can be seen by comparing Tables 6.2 and 6.2.

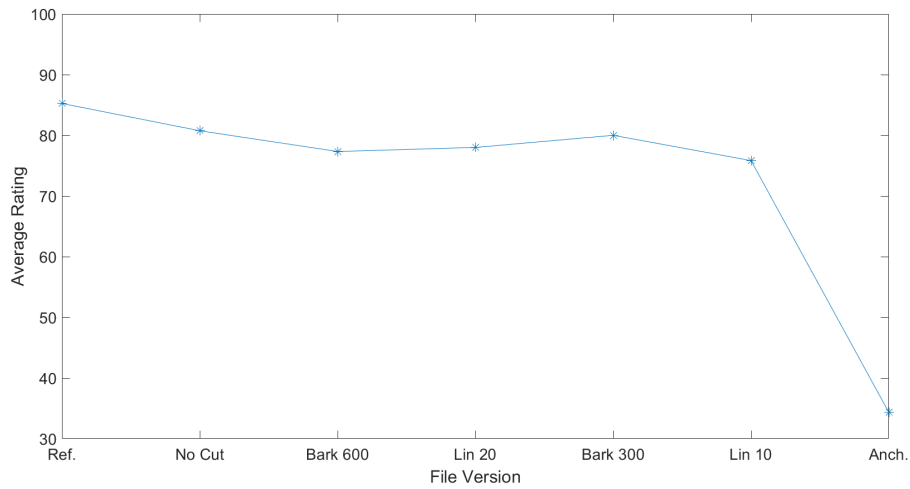


**Figure 6.5:** Average ratings for the guitar samples. From left to right: Hidden Reference, No Cut, Bark 600, Linear 20, Bark 300, Linear 10, Anchor.

### Guitar Samples

The results obtained with the guitar samples, depicted in Figure 6.5 are more uniform. Again, the anchor was correctly recognised and, this time, so were the hidden reference and the No Cut versions, which got the highest ratings. In spite of this, the Bark 300 version obtained a surprisingly good result again, this time even higher than the Bark 600. While the latter fact might be due to some bias, this is still a confirm of the good quality of the Bark optimisation.

### Vocals Samples

The vocals samples average ratings are illustrated in Figure 6.6; it is possible to observe how, again, the anchor was correctly recognised. This time, however, it is clearly visible how both the linear optimised versions got really low ratings. Such a result cannot be justified only by a bias in the test, and means that the linear optimisation introduced some strange artifacts, particularly evident in the vocals samples. The ratings obtained by the other samples are another confirm of the good quality of the Bark optimisation.

## 6.5 Final Considerations

The results of both the technical evaluation and the perceptual test indicate that the optimisation technique implemented is able to maintain a high grade of quality with respect to the original sound while, the same time, allowing for a drastic

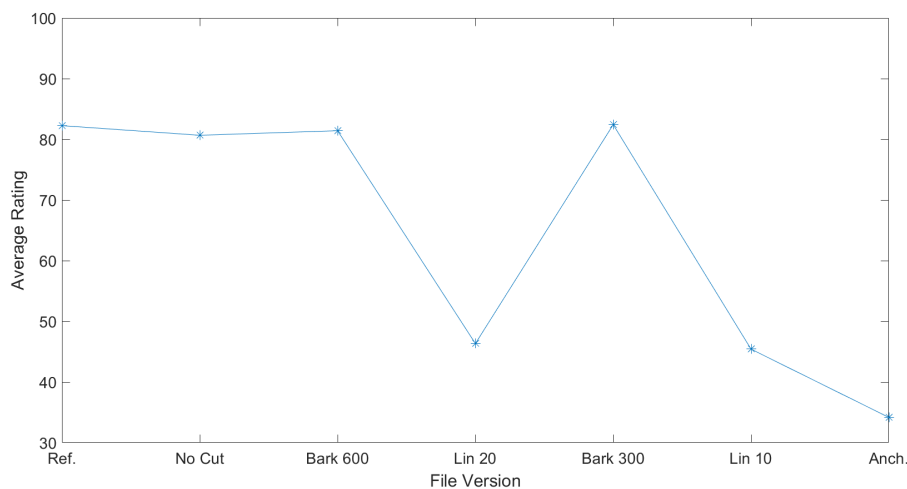


**Figure 6.6:** Average ratings for the vocals samples. From left to right: Hidden Reference, No Cut, Bark 600, Linear 20, Bark 300, Linear 10, Anchor.

reduction of the computational power requested by the plate for running, as reported in Table 6.1. In addition, the outcome of the two experiments show that the Bark scale is probably the best way for dividing the frequency axis when performing the least squares optimisation. In fact, the audio files processed this way obtained the best results in terms of both correlation coefficient and perceptual rating, while still requiring at least 80% of time less to compute with respect to the non-optimised version of the plate. These results also indicate that the overall correlation coefficient, if accompanied by psychoacoustic considerations, is a reliable indicator for measuring the differences between two frequency responses.

In the last question, in which subjects had to provide their personal opinion on the reverberation effect, the comments were generally positive, nevertheless, the majority of them stressed the fact that the effected sound was too wet. This is true indeed, in fact, it is very rare to use a reverb in a completely wet mode. In spite of this, it was decided not to mix the wet and dry sounds to let the testers focus on completely on the reverberation effect. In the context of a practical use of the plate simulation, this would be used for sure with a wet/dry control, for deciding how much reverb to introduce. Nevertheless, as previously mentioned, further testing need to be conducted to test the overall sound quality of the plate model.



## Chapter 7

# Conclusion & Future Work

In this work, a physical model of an EMT 140 plate reverb was implemented with MATLAB and presented, along with an optimisation technique which allows to reduce the computational time. In particular, the algorithm includes a physically-based damping, with two damper models, several materials, an exact numerical integrator for solving the modes equation and an optimisation techniques based on linear least squares, which allows to analyse the frequency spectrum in linear or Bark bands. An evaluation was performed, which indicated that the Bark scale is the best way for analysing the plate, and that the optimisation allows to reduce the computational time by the 80% without affecting too much the sound quality. Not having a real EMT 140 at hand made it impossible to perform a sound comparison for understanding if the simulation is actually capable of accurately emulating the plate. Nonetheless, the overall opinions on the reverb given by the testers were positive.

In the future, many improvements could be performed on the model. The first and most obvious would focus on building a real time plugin with the C++ language. As previously mentioned, since it allows to work at a lower level, the use of this programming language would speed up the computation even more, allowing to run the stereo version of the plugin in real-time. Possible further work include a more accurate model for the damper, based on measurements on a real EMT 140 device, and the formalisation of a spatial extended punctual actuator. In fact, at the moment, the exciter is considered being concentrated on one spatial point, and modeled with a Dirac delta, while in the real case it has a spatial extension. Another improvement would involve to link the damper position to the  $T_{60}$ , thus providing a control similar to the one present on the real device, which indicates the decay time at 500 Hz. Having an actual EMT 140 unit at hand to measure would allow to perform a comparison with the algorithm sound. This would also make possible to better tune the optimisation, by finding several fixed values for the maximum modes limit for choosing between sound quality and performances.



# Bibliography

- [1] Vesa Välimäki et al. "More Than 50 Years of Artificial Reverberation". In: *Proc. 60th International Conference of the Audio Engineering Society*. Ed. by Stefan Goetze and Ann Spriet. United States: Audio Engineering Society, 2016.
- [2] Kevin Arcas Castillo. "Simulation numérique d'un réverbérateur à plaque". Theses. Ecole Polytechnique X, Apr. 2009.
- [3] H. J. Round and A.G.D West. "Transmission and Reproduction of Sound". Pat. US1853286A. 1932.
- [4] R. L. Wegel. "Wave Transmission Device". Pat. US1852795A. 1932.
- [5] Soundonsound. *Plate Reverb Image*. Accessed: 2021-05-07. URL: [www.soundonsound.com/techniques/mechanical-sfx](http://www.soundonsound.com/techniques/mechanical-sfx).
- [6] James Rotondi. *Tips and Tricks - EMT 140 Classic Plate Reverberation Plugin*. Accessed: 2021-05-23. URL: [www.uaudio.com/blog/emt-140-tips-and-tricks](http://www.uaudio.com/blog/emt-140-tips-and-tricks).
- [7] Schmitz Sabine. "Collected Papers on Acoustics". In: *Harvard University Press* (1922). DOI: 10.1121/1.2221392.
- [8] Leo Beranek. "Analysis of Sabine and Eyring equations and their application to concert hall audience and chair absorption". In: *The Journal of the Acoustical Society of America* 120 (Oct. 2006), pp. 1399–1410. DOI: 10.1121/1.2221392.
- [9] Karolina Prawda, Sebastian J. Schlecht, and Vesa Välimäki. "Evaluation of Reverberation Time Models with Variable Acoustics". In: *Proceedings of the 17th Sound and Music Computing Conference*. Torino, Italy, 2020, pp. 145–152.
- [10] M.R. Schroeder and B.F. Logan. "'Colorless' artificial reverberation". In: *IRE Transactions on Audio* AU-9.6 (1961), pp. 209–214. DOI: 10.1109/TAU.1961.1166351.
- [11] R. Schroeder M. "natural sounding artificial reverberation". In: *journal of the audio engineering society* 10.3 (1962), pp. 219–223.
- [12] James Moorer. "About This Reverberation Business". In: vol. 3. Jan. 1985, pp. 605–639. ISBN: 978-0262680516. DOI: 10.2307/3680280.

- [13] John Stautner and Miller Puckette. "Designing Multi-Channel Reverberators". In: *Computer Music Journal* 6.1 (1982), pp. 52–65. issn: 01489267, 15315169. URL: <http://www.jstor.org/stable/3680358>.
- [14] Jean-Marc Jot and Antoine Chaigne. "Digital Delay Networks for Designing Artificial Reverberators". In: *Audio Engineering Society Convention 90*. 1991. URL: <http://www.aes.org/e-lib/browse.cfm?elib=5663>.
- [15] Sebastian J. Schlecht and Emanuël A. P. Habets. "On Lossless Feedback Delay Networks". In: *IEEE Transactions on Signal Processing* 65.6 (2017), pp. 1554–1564. DOI: 10.1109/TSP.2016.2637323.
- [16] Karolina Prawda, Vesa Välimäki, and Sebastian Schlecht. "Improved Reverberation Time Control for Feedback Delay Networks". In: *Proceedings of the 22nd International Conference on Digital Audio Effects, DAFX*. Birmingham, U.K., Sept. 2019.
- [17] Sebastian Schlecht and Emanuël Habets. "Reverberation enhancement from a feedback delay network perspective". In: Nov. 2012. DOI: 10.1109/EEEI.2012.6376933.
- [18] Jonathan S. Abel, David P. Berners, and Aaron Greenblatt. "An Emulation of the EMT 140 Plate Reverberator Using a Hybrid Reverberator Structure". In: *Audio Engineering Society Convention 127*. 2009.
- [19] Andrew Reilly and David McGrath. "Convolution Processing for Realistic Reverberation". In: *Audio Engineering Society Convention 98*. 1995.
- [20] William G. Gardner. "Efficient Convolution without Input-Output Delay". In: *J. Audio Eng. Soc* 43.3 (1995), pp. 127–136.
- [21] Shinichi Sakamoto et al. "Calculation of Impulse Responses and Acoustic Parameters in a Hall by the Finite-Difference Time-Domain Method". In: *Acoustical Science and Technology* 29.4 (2008), pp. 256–265. DOI: 10.1250/ast.29.256.
- [22] L. Savioja, T. Rinne, and Tapio Takala. "Simulation of Room Acoustics with a 3-D Finite Difference Mesh". In: *The 1994 International Computer Music Conference, Aarhus, September 12-17, 1994*. Int. Computer Music Ass. and Danish Inst. of Electroa. Music, 1994, pp. 463–466.
- [23] Julius O. Smith. "Physical Modeling Using Digital Waveguides". In: *Computer Music Journal* 16 (1992), p. 74.
- [24] D.T. Murphy et al. "Acoustic Modeling Using the Digital Waveguide Mesh". In: *Signal Processing Magazine, IEEE* 24 (Apr. 2007), pp. 55–66. DOI: 10.1109/MSP.2007.323264.

- [25] Damian T. Murphy, Chris J. C. Newton, and David M. Howard. “Digital Waveguide Mesh Modelling of Room Acoustics: Surround-Sound Boundaries and Plugin Implementation”. In: *Proceedings of the Cost G-6 Conference on Digital Audio DAFX-168 Effects (DAFX-01)*. 2001, pp. 198–202.
- [26] Cumhur Erkut and Karjalainen Matti. “Digital Waveguides versus Finite Difference Structures: Equivalence and Mixed Modeling”. In: *EURASIP Journal on Advances in Signal Processing* 2004 (June 2004). doi: 10.1155/S1110865704401176.
- [27] Cumhur Erkut and Matti Karjalainen. “Finite Difference Method vs. Digital Waveguide Method in String Instrument Modeling and Synthesis”. In: *Proceedings of the International Symposium on Musical Acoustics (ISMA-02), Mexico City, 2002* (Sept. 2002).
- [28] Antoine Chaigne and Christophe Lambourg. “Time-domain simulation of damped impacted plates. I. Theory and experiments”. In: *The Journal of the Acoustical Society of America* 109 (May 2001), pp. 1422–1432. doi: 10.1121/1.1354200.
- [29] Christophe Lambourg, Antoine Chaigne, and Denis Matignon. “Time-domain simulation of damped impacted plates. II. Numerical model and results”. In: *The Journal of the Acoustical Society of America* 109.4 (2001), pp. 1433–1447. doi: 10.1121/1.1354201.
- [30] S. Bilbao, Kevin Arcas, and A. Chaigne. “A Physical Model for Plate Reverberation”. In: *2006 IEEE International Conference on Acoustics Speech and Signal Processing Proceedings* 5 (2006).
- [31] Kevin Arcas. “Physical Modelling and Measurements of Plate Reverberation”. In: *in Proceedings of the ICA*. 2007.
- [32] Michele Ducceschi and Craig J. Webb. “Plate reverberation: Towards the Development of a Real-Time Physical Model for the Working Musician”. In: *Proceedings of the 22nd International Congress on Acoustics ICA*. Proceedings of the ICA Congress. Buenos Aires, Argentina, Sept. 2016.
- [33] Silvin Willemsen, Stefania Serafin, and Jesper Rindom Jensen. “Virtual Analog Simulation and Extensions of Plate Reverberation”. In: *Proceedings of the 14th Sound and Music Computing Conference*. 2017, pp. 314–319.
- [34] Marco A. Martínez Ramírez and Joshua D. Reiss. “Modeling Nonlinear Audio Effects with End-to-end Deep Neural Networks”. In: *Proc. IEEE International Conference on Acoustics, Speech and Signal Processing, ICASSP 2019, Brighton, United Kingdom*. May 2019, pp. 171–175.

- [35] Marco A. Martinez Ramirez, Emmanouil Benetos, and Joshua D. Reiss. "Modeling Plate and Spring Reverberation Using A DSP-Informed Deep Neural Network". In: *ICASSP 2020 - 2020 IEEE International Conference on Acoustics, Speech and Signal Processing (ICASSP) (2020)*. DOI: 10.1109/icassp40776.2020.9053093.
- [36] Universal Audio. *EMT 140 Classic Plate Reverberator*. Accessed: 2021-05-09. URL: [www.uaudio.com/uad-plugins/reverbs/emt-140.html](http://www.uaudio.com/uad-plugins/reverbs/emt-140.html).
- [37] IK Multimedia. *CSR Plate Reverb*. Accessed: 2021-05-09. URL: [www.ikmultimedia.com/products/trcsrplate](http://www.ikmultimedia.com/products/trcsrplate).
- [38] Waves Audio. *Abbey Road Reverb Plates*. Accessed: 2021-05-09. URL: [www.waves.com/plugins/abbey-road-reverb-plates#abbey-road-reverb-plates-plugin-audio-demos](http://www.waves.com/plugins/abbey-road-reverb-plates#abbey-road-reverb-plates-plugin-audio-demos).
- [39] Arturia. *Rev PLATE-140*. Accessed: 2021-05-17. URL: [www.arturia.com/products/software-effects/reverbs-bundle/rev-plate140](http://www.arturia.com/products/software-effects/reverbs-bundle/rev-plate140).
- [40] ValhallaDSP. *Valhalla Plate*. Accessed: 2021-05-09. URL: [valhallaDSP.com/shop/reverb/valhalla-plate](http://valhallaDSP.com/shop/reverb/valhalla-plate).
- [41] David Baer. *Valhalla Plate from ValhallaDSP Review*. Accessed: 2021-05-09. 2015. URL: [soundbytesmag.net/valhallaplatefromvalhallaDSP](http://soundbytesmag.net/valhallaplatefromvalhallaDSP).
- [42] Physical Audio. *PA1 Dynamic Plate Reverb*. Accessed: 2021-05-09. URL: [www.uvi.net/plate.html](http://www.uvi.net/plate.html).
- [43] UVI. *UVI Plate*. Accessed: 2021-05-09. URL: [www.uvi.net/plate.html](http://www.uvi.net/plate.html).
- [44] Karl Graff. *Wave Motion in Elastic Solids*. New York, NY, USA: Dover Publications Inc., 1975.
- [45] Stefan Bilbao. *Numerical Sound Synthesis*. Chichester, UK: John Wiley & Sons, Ltd, 2009. ISBN: 9780470749012.
- [46] Stefan Bilbao and Maarten Van Walstijn. "A Finite Difference Plate Model". In: Jan. 2005, pp. 119–122.
- [47] Kevin Arcas and Antoine Chaigne. "On the quality of plate reverberation". In: *Applied Acoustics* 71.2 (2010), pp. 147–156. ISSN: 0003-682X. DOI: <https://doi.org/10.1016/j.apacoust.2009.07.013>.
- [48] Yiwei Kou, Bilong Liu, and Jing Tian. "Radiation efficiency of damped plates". In: *The Journal of the Acoustical Society of America* 137.2 (2015), pp. 1032–1035. DOI: 10.1121/1.4906186.
- [49] M.A. Kenawy, M.Y. Elaidy, and Mohammed Abd-Elbasseer. "Theoretical determination of critical frequency  $f_c$  of some acoustic material panels". In: *12th International Congress on Sound and Vibration 2005, ICSV 2005 2* (Jan. 2005), pp. 1530–1537.

- [50] Gideon Maidanik. "Response of Ribbed Panels to Reverberant Acoustic Fields". In: *The Journal of the Acoustical Society of America* 34.6 (1962), pp. 809–826. DOI: 10.1121/1.1918200.
- [51] A. Cummings, H.J Rice, and R. Wilson. "Radiation Damping in Plates, Induced by Porous Media". In: *Journal of Sound and Vibration* 221.1 (1999), pp. 143–167. ISSN: 0022-460X. DOI: <https://doi.org/10.1006/jsvi.1998.1987>.
- [52] D. Tomlinson, R.J.M. Craik, and R. Wilson. "Acoustic Radiation from a Plate into a Porous Medium". In: *Journal of Sound and Vibration* 273.1 (2004), pp. 33–49. ISSN: 0022-460X. DOI: <https://doi.org/10.1016/j.jsv.2003.04.003>.
- [53] A. Cummings. "Sound Radiation from a Plate into a Porous Medium". In: *Journal of Sound and Vibration* 247.3 (2001), pp. 389–406. ISSN: 0022-460X. DOI: <https://doi.org/10.1006/jsvi.2000.3736>.
- [54] Leonard Meirovitch. *Fundamentals of Vibrations*. New York, NY, USA: McGraw-Hill, 2001.
- [55] Lawrence E. Kinsler et al. *Fundamentals of Acoustics, 4th Edition*. Hoboken, NJ, USA: Wiley, 1999.
- [56] Esteban Maestre and J. O. Smith. "Constrained Pole Optimization for Modal Reverberation". In: Edinburgh, UK, 2017, pp. 381–388.
- [57] S.A. Ryder. "Methods for Comparing Frequency Response Analysis Measurements". In: *Conference Record of the the 2002 IEEE International Symposium on Electrical Insulation (Cat. No.02CH37316)*. 2002, pp. 187–190. DOI: 10.1109/ELINSL.2002.995909.
- [58] The ITU Radiocommunication Assembly. *Method for the subjective assessment of intermediate quality level of coding systems*. Accessed: 2021-05-21. URL: [www.itu.int/dms\\_pubrec/itu-r/rec/bs/R-REC-BS.1534-1-200301-S!PDF-E.pdf](http://www.itu.int/dms_pubrec/itu-r/rec/bs/R-REC-BS.1534-1-200301-S!PDF-E.pdf).
- [59] G. Stoet. "PsyToolkit - A software package for programming psychological experiments using Linux". In: *Behavior Research Methods* 42.4 (2010), pp. 1096–1104.
- [60] G. Stoet. "PsyToolkit: A novel web-based method for running online questionnaires and reaction-time experiments". In: *Teaching of Psychology* 44.1 (2017), pp. 24–31.